

Design and Fabrication of Magnetic Elastomer-Based Soft Actuator

2022 CNF REU Intern: Rodolfo Cantu

Intern Affiliation: Mechanical Engineering,
The University of Texas at Austin

CNF REU Principal Investigator: Dr. Amal El-Ghazaly, Electrical and Computer Engineering, Cornell
CNF REU Mentor: Ludovico Cestarollo, Electrical and Computer Engineering, Cornell University
CNF REU Project and Primary Source(s) of Research Funding: 2022 Cornell NanoScale Science
& Technology Facility Research Experiences for Undergraduates (CNF REU) Program
via the National Science Foundation under Grant No. NNCI-2025233

Contact: rodolfo.cantu@utexas.edu, ase63@cornell.edu, lc942@cornell.edu

Website: <https://cnf.cornell.edu/education/reu/2022>

Primary CNF Tools Used: ABM Contact Aligner, Heidelberg Mask Writer - DWL2000,
AJA Ion Mill, Plasma-Therm 72, P7 Profilometer, AFM Bruker Icon

Abstract:

Technological advancements to date have primarily focused on stimulating only two of the five human senses: sight and hearing. Touch-based interactive technologies are still in their infancy. Haptic devices allow tactile interactions between humans and digital interfaces, assisting humans in industries such as healthcare, automotive and entertainment. Magnetorheological elastomers (MREs) based on nanoparticles constitute a promising candidate material for creating tactile interfaces [1] capable of creating high-resolution features on the micron scale [2]. These magneto-responsive elastomers must be integrated with magnetic micro-controls to create the local magnetic fields necessary to actuate deformations.

Summary of Research:

The future of touch-based haptic interfaces relies on the actuation of microscale thin films. Magneto-responsive soft-actuators have the potential to create low-power, high-responsivity, and low-cost haptic interfaces. A process was developed to create a system of micromagnetic controls integrated into microscale beams made of an MRE. This project is structured into three main objectives: the fabrication and characterization of magnetic microcontrols, the fabrication of a micrometer thin MRE, and the integration of actuation controls and MRE.

The design concept involves two micromagnetic controls on the surface of an MRE thin film (see Figure 1). The MRE is constituted of a soft silicone rubber matrix and magnetic nanoparticles forming vertical chains in the thickness direction of the film. The micro controls are made of pillars with circular and elliptical base. The circular magnets (perpendicular magnetic



Figure 1: Device design of magnetorheological elastomer with two integrated magnetic micro controls.

anisotropy (PMA) magnets) are fabricated so that the magnetic moment lies preferentially in the direction perpendicular to their surface. The elliptical magnets (in-plane magnetic anisotropy (IMA) magnets) are deposited to be magnetized in the direction of the long axis. When the controls are embedded into the MRE, their magnetic fields will couple and interact with the elastomer in proximity of the gap between them, causing it to deflect.

The first step in the creation of this device is the fabrication of the magnets. Starting with a 4-inch clean silicon wafer, 350 nm

of LOR3A and 450 nm of S1805 (positive) resist were spin coated, following with a soft bake at 180°C for five minutes for the former and at 115°C for one minute for the latter. The coated wafer was then exposed in an ABM contact aligner for 1.5 seconds and developed for 60 seconds using 726 MIF solvent. The patterned wafer was then descummed with oxygen plasma for 60 seconds

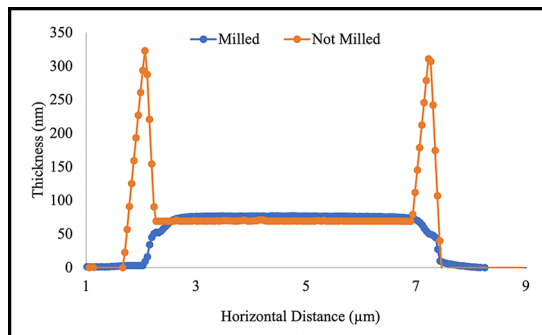


Figure 2: Ion milling to remove “rabbit ears” resulting from sputtering and lift-off.

with oxygen flow of 30 sccm and 50 W of power. Then the magnets were deposited via sputtering.

The elliptical pillars were constituted of 3 nm of Ta, 5 nm of Pt, 58 nm of Co, and 5 nm of Pt. The circular pillars were sputtered with 19 alternating layers of Co (1 nm) and Pt (2 nm) and a final 1 nm layer of Co, using the same Ta/Pt underlayer and Pt capping layer as for the elliptical magnets. After sputtering, the wafer was soft baked at 115°C to facilitate the lift-off process, which was performed by first hitting the wafer with pressurized solvents at 1600 psi (C&D SmartProP9000), and submerging it in Remover 1165 for 20 minutes. Finally, an AJA milling tool was used at 600 V for 120 seconds with a 5° tilt to eliminate the “rabbit ears” caused by sputtering and lift-off (see Figure 2).

At this stage, the wafer was diced into 10 × 10 mm devices, each presenting specific geometry and dimensions. The magnetic properties of the deposited magnets were studied via vibrating sample magnetometry (VSM) and the optimal dimensions for both geometries were identified. The hysteresis loops obtained with VSM illustrate the magnetic properties of a magnetic sample, allowing to extract coercivity and remanent magnetization values. The circular pillars, with diameters ranging from 3 to 100 μm were tested for their magnetization in response to an out-of-plane applied magnetic field (see the hysteresis loops in Figure 3). The elliptical samples with in-plane magnetization were measured along both the short and long axes, as shown in Figure 4. The optimal magnetic properties were found in the 5 μm diameter circular magnet (maximum remanent magnetization and coercivity) and the 3 μm (short axis), 15 μm (long axis) elliptical magnet (largest difference between hysteresis loop measured along the two axes). Atomic force microscopy (AFM) was used to confirm the dimensions of the deposited geometries.

Finally, a system of micromagnets (one IMA and PMA magnet spaced apart 1, 1.5 and 2 μm) was ultimately designed to be integrated into cantilevers and simply supported beams made of a micrometer-thin MREs to create a magnetic soft actuator. the elastomer was

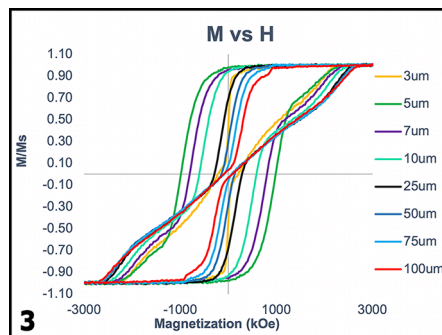


Figure 3: Magnetic hysteresis loops for PMA circles.

composed of 95 wt% Sylgard 527 and 5 wt% Sylgard 184. After mixing the two elastomers using a vortex for a few seconds, 6 vol% of Fe nanoparticles were added and mixed for about 3 minutes. The dispersion was homogenized for 1 hour and 15 minutes using an ultrasonicating bath. Finally, the mix was spin coated on a wafer at 7500 rpm for 60s to achieve a thickness of 2-2.5 μm.

Conclusions and Future Steps:

We demonstrated the fabrication process of micro-magnets and discussed their optimal dimensions to achieve desired magnetic properties. Magnetic simulations carried out in our lab guided the choice of a reasonable spacing between the IMA and PMA magnets when integrated into the soft actuator. Next, the developed controls will need to be embedded into cantilevers and beams with the actuation performance assessed. We believe these results serve as a foundation for the fabrication of soft magnetorheological elastomers with integrated magnetic controls.

References:

- [1] Böse, H., et al. Magnetorheological Elastomers - An Underestimated Class of Soft Actuator Materials. *Journal of Intelligent Material Systems and Structures* (2021).
- [2] L. Cestarollo, et al. Nanoparticle-based magnetorheological elastomers with enhanced mechanical deflection for haptic displays, *ACS Applied Materials and Interfaces* 14 (2022),

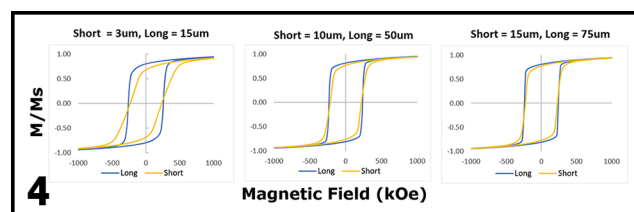


Figure 4, bottom: Magnetic hysteresis loops for short and long axis of IMA ellipses.

Investigating the Electrokinetic Behavior of Cement-Based and Alternative Cementitious Materials

2022 CNF REU Intern: Rachel Qian

Intern Affiliation: Chemical Engineering, Villanova University

CNF REU Principal Investigator: Dr. Sriramy Nair, Civil and Environmental Engineering, Cornell
CNF REU Mentor: Lyn Zemberekci, Civil and Environmental Engineering, Cornell University
CNF REU Project and Primary Source(s) of Research Funding: 2022 Cornell NanoScale Science & Technology Facility Research Experiences for Undergraduates (CNF REU) Program via the National Science Foundation under Grant No. NNCI-2025233

Contact: rqian@villanova.edu, sn599@cornell.edu, lz549@cornell.edu

Website: <https://cnf.cornell.edu/education/reu/2022>

Primary CNF Tools Used: Malvern Zetasizer, Scanning Electron Microscope

Abstract:

Portland cement production is a major contributor of carbon dioxide emissions, The need to incorporate large amounts of Supplementary Cementitious Materials (SCMs) to reduce the carbon footprint arises. Various SCMs were dispersed in diluted pore solutions that mimic native pore solutions of cement pastes characterized by their high pH and ionic nature. Chemical additives such as sodium glucoheptonate retarders and naphthalene sulfonate-based superplasticizers were employed to track their efficacy with the SCMs. Electrokinetic properties such as zeta potential was of primary interest in this study to ensure cement pastes have adequate rheological properties. Factors that influenced zeta potential such as electrical conductivity and pH were also measured in optimized particle solid concentrations. Stable zeta potentials have an absolute value measurement of 30 mV or above. Without the use of admixtures, it was found that majority of the particles were unstable and tended to aggregate in the pore solutions, with zeta potential values ranging from -3.13 mV to 11.5 mV. Silica flour displayed the most stable behavior in the diluted pore solution concentration, with a zeta potential around -22 mV. The use of chemical additives led to increases in the zeta potential values as compared to those of the neat particles, demonstrating that the additives are compatible with some of the particles and effective in improving the stability of the solution. Furthermore, scanning electron microscope imaging was used to view the shape and size of the cementitious particles as these factors also affect the rheology of the cementitious paste.

Summary of Research:

This research aimed at characterizing the electrokinetic behavior of Supplementary Cementitious Materials (SCMs), such as silica flour (SFL), class F fly ash (FAF), class C fly ash (FAC), metakaolin (MK) and ground granulated blast-furnace slag (SLAG) in DI water and pore solutions. Additionally, class H cement (CEM-H) was also analyzed as a baseline. To study the electrokinetic behavior, zeta potential values were tracked using a zetasizer, Malvern Instrument. $800 \mu\text{L}$ of these neat (in the absence of chemical additives) pore solutions was injected into a reusable cuvette, which was then placed into the zetasizer. The zetasizer measured the sample's electrophoretic mobility at six measurements per sample and used the Smoluchowski approach to calculate the zeta potential values.

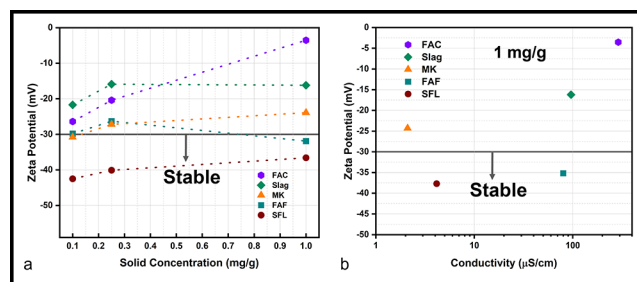


Figure 1: (a) Zeta potential values of various SCM particles with increasing solid concentration in deionized water, (b) Zeta potential vs. conductivity for one concentration.

We found that SFL had most stable behavior in DI water, with zeta potential values above 30 mV for all concentrations. FAC experienced aggregation, which was attributed to the pH and conductivity of the solution. After graphing zeta potential vs. conductivity, it was found that as conductivity increased, the zeta potential decreased, and solutions became less stable. These trends are summarized in Figure 1.

Then we used a synthesized pore solution made up of 0.6 g/L calcium sulfate dehydrate, 5.2 g/L sodium hydroxide, 17.9 g/L potassium hydroxide, and 2.4 g/L calcium hydroxide with a pH of 13.5 to test our SCMs and class H cement particles. Pore solution concentration used was 25 mL pore solution / 375 mL DI water. We mixed 100 mL of this diluted solvent with 100 mg particles through a 15-minute sonication.

Particle	Zeta Potential (mV)	pH	Conductivity (mS/cm)
Class H Cement (CEMH)	4.5	12.4	7.5
Silica Flour (SFL)	-22.0	12.2	7.2
Class F Fly Ash (FAF)	-3.1	12.1	6.9
Metakaolin (MK)	1.4	12.1	7.6
Class C Fly Ash (FAC)	2.2	12.1	6.8
Slag	12.0	12.2	8.0

Table 1: Electrokinetic behavior of various SCMs and class H cement in pore solution.

As shown in Table 1, it was found that majority of the particles became unstable and tended to aggregate in the pore solutions, with zeta potential values ranging from -3.13 mV to 11.5 mV. SFL displayed the most stable behavior in the diluted pore solution concentration, with a zeta potential around -22 mV. The use of chemical additives such as sodium glucoheptonate (SGH) and naphthalene-based superplasticizers led to increases in the zeta potential values of the CEM-H as compared to those without any additives, demonstrating that the additives are compatible and effective in improving the stability of the solution. However, these increases were bounded by certain concentrations of additives. This is illustrated in Figures 2 and 3.

Conclusions and Future Steps:

Zeta potential values of SCMs such as MK and FAF were similar to those found in literature [1-3], validating the procedure of this study. Majority of SCMs exhibited stable behavior when using deionized water as a solvent, apart from FAC.

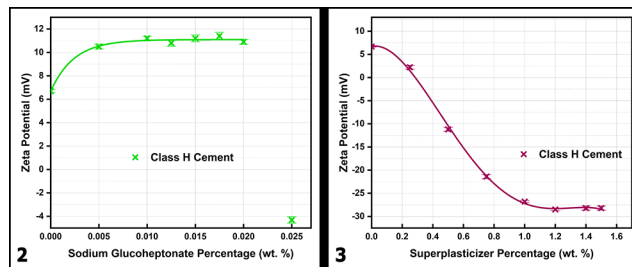


Figure 2, left: Zeta potential values of class H cement in pore solution with an increasing content of the retarder sodium glucoheptonate. Figure 3, right: Zeta potential values of class H cement in pore solution with an increasing content of the naphthalene-based superplasticizer.

Opposite was true when using pore solution as a solvent, except for SFL. CEM-H interactions with the retarding additive SGH in the pore solution indicated that this additive improves the stability of the solution to a certain point, after which increasing the SGH content results in aggregation. CEM-H in the presence of the superplasticizer additive showed that stability of the solution increased up to a saturation point, after which there is no significant effect.

To observe aggregation of particles, along with measuring zeta potential we will also measure the particle size of each of the SCMs. This will be achieved by adding an additional sieving and filtering process to limit particle sizes to 5 μm . We will also aim at conducting adsorption tests of polymer-based additives onto the SCM particles using an ultraviolet-visible (UV-vis) light device. In future experiments, there will be further optimization of pH and conductivity versus zeta potential.

References:

- [1] Malta, J. O., Oliveira, L. V., Ueki, M. M., and Barreto, L. S. (2021). Characterization and stabilization of nano-metakaolin colloidal suspensions. *Powder Technology*, 383, 43-55.
- [2] Malek, R. I., Khalil, Z. H., Imbaby, S. S., and Roy, D. M. (2005). The contribution of class-F fly ash to the strength of cementitious mixtures. *Cement and concrete research*, 35(6), 1152-1154.
- [3] Wang, C., Kayali, O., and Liow, J. L. (2021). The effectiveness and mechanisms of superplasticisers in dispersing class F fly ash pastes. *Powder Technology*, 392, 81-92.

Access to Porous Substructure of Block Copolymer-Derived Nanomaterials via Reactive Ion Etching (RIE)

CNF Project Number: 1356-05

Principal Investigator(s): Ulrich Wiesner

User(s): Fei Yu

Affiliation(s): Department of Materials Science and Engineering, Cornell University

Primary Source(s) of Research Funding: U.S. Department of Energy (DOE),

Office of Science (Basic Energy Sciences (DE-SC0010560))

Contact: ubw1@cornell.edu, fy84@cornell.edu

Website: <http://wiesner.mse.cornell.edu/>

Primary CNF Tools Used: Oxford 81 Etcher

Abstract:

The use of block copolymers (BCPs) as structure-directing agent offers a facile pathway toward nanomaterials with tunable mesostructures and functional properties. However, the surface energy often disrupts the thermodynamics of block copolymer self-assembly and results in a different surface morphology from the bulk substructure. In this report, we demonstrate the use of reactive ion etching (RIE) in the CNF cleanroom as a simple technique to access the substructure in block copolymer-derived carbon materials. RIE removes the dense capping layer on the surface so that we can make use of the internal structure with massive meso- and nano-porous surface areas. These carbon monoliths with open pore structures may be promising candidates for electrode materials in the design of 3D continuous electrochemical energy storage devices.

Summary of Research:

With high interfacial areas and a low areal footprint, three-dimensionally (3D) continuous nanostructured electrode materials have gained interest as the demand for increasingly efficient electrochemical energy storage devices grows. As a result, nanostructured carbon materials with 3D network architectures are under active investigation for routes to 3D functional composite materials, e.g., via straightforward backfilling, for the eventual incorporation into energy storage devices.

In our work, ultralarge molar mass diblock copolymers are employed as structure-directing agents for carbon precursors to prepare carbons with ultralarge pore sizes. The unfavorable interaction between the large blocks forces them to segregate from each other at the nanoscale and the carbon precursors preferentially mix with the more hydrophilic block. Upon heat treatment in the furnace to high temperatures of up to 1600°C, nonperiodically ordered co-continuous network structures are derived with an average pore sizes of around 100 nm (Figure 1).

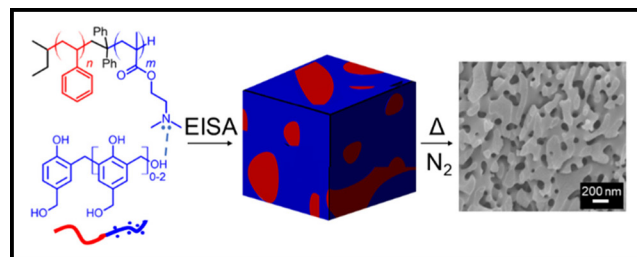


Figure 1: Schematic of the self-assembly of BCPs and carbon precursors (left) via evaporation-induced self-assembly (EISA) into mesostructured hybrids (middle) and the mesoporous carbon materials after high-temperature treatments (right). The SEM images show representative cross sections of the final monoliths.

After subsequent carbon activation processes, the porous carbons with continuous 3D network structures are a promising candidate as the cathode materials for the intercalation of lithium. However, since the self-assembled mesostructures are formed from a solution in

a dish, the solution-air and solution-container interfaces experience different thermodynamic driving forces for the microphase segregation of the BCPs. The scanning electron microscopy (SEM) image in Figure 2a shows that the surface of an as-made hybrid that has gone through the heat treatment is capped by a dense layer, which renders the porous understructure inaccessible.

In order to realize the potential of the porous 3D network structure, Oxford 81 Etcher was utilized with oxygen plasma. Each side of the as-made hybrid is subject to 30 min of oxygen plasma at 150 W forward power, 50 sccm flow rate, and 60 mTorr pressure. Figure 2b shows the carbon structure derived from heat treating the etched hybrid, whose underlying pores in the substructure are now fully accessible from the surface.

Conclusions and Future Steps:

In summary, a one-pot route to co-continuous porous carbons is demonstrated via ultralarge molar mass block polymer self-assembly with carbon precursors. Aided by reactive ion etching (RIE), open and accessible 3D co-continuous pore network structures of carbon materials make them appealing for applications that require fast kinetics through the large 3D continuous pore network or backfilling processes, e.g., required for producing 3D nanoarchitecture-based energy storage devices.

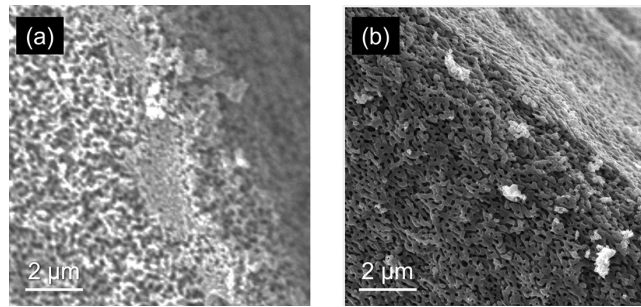


Figure 2: Scanning electron microscopy (SEM) images of carbon monoliths derived from heat treating BCP-carbon precursor hybrids (a) without and (b) with oxygen plasma etching.

References:

- [1] Tait, W.R., Thedford, R.P., Chapman, D.V., Yu, F., Freidl, J.W., Sablina, E.S., Batsimm, G.M. and Wiesner, U.B. One-Pot Structure Direction of Large-Pore Co-Continuous Carbon Monoliths from Ultralarge Linear Diblock Copolymers. *Chemistry of Materials* 2021, 33(19), 7731-7742.

Autonomous High-Throughput Materials Discovery of Metal Oxide Thin Films via Laser Spike Annealing, Spatially Resolved X-Ray Diffraction, and Thin Film Device Characterization

CNF Project Number: 1400-05

Principal Investigator(s): R. Bruce van Dover

User(s): Duncan Ross Sutherland

Affiliation(s): Materials Science and Engineering, Cornell University

Primary Source(s) of Research Funding: Air Force Research Laboratory FA9550-18-1-0136,
Cornell NanoScale and Science and Technology Facilities NNCI-2025233,
Cornell High Energy Synchrotron Source DMR-1332208

Contact: vandover@cornell.edu, drs378@cornell.edu

Primary CNF Tools Used: CHA Thermal Evaporation, General Photolithography Equipment,
Developing Tools, Mask Writers, Wafer Scale Tube Furnaces, Some Metrology Equipment

Abstract:

The study of complex oxides through combinatorial efforts would require a prohibitive amount of material resources and time if experiments were conducted using bulk techniques and at macroscopic length scales. We employ leading edge materials processing in conjunction with advanced micron-scale synchrotron characterization to enable these high-throughput studies and accelerate materials optimization and discovery. This research area is additionally enhanced by incorporating artificial intelligence and machine learning methods. Dimensionality reduction and reproducibility of the processing techniques requires a precision registration of the micron-scale x-ray characterization is essential for analytical autonomous research. We use the Cornell NanoScale and Science and Technology Facilities (CNF) in order to align each of the experimental elements with a primary goal of discovering novel materials. Thin film capacitor devices are constructed post material processing to allow electrical characterization of the properties of the materials synthesized.

Summary of Research:

The focus of the van Dover research group is combinatorial and autonomous materials exploration via thin film synthesis, processing, and characterization. The scale of possible material combinations becomes exponentially large for thin films with a composition spread spanning multiple degrees of chemical freedom, and processing adds even more dimensions of complexity. While exhaustive searching of a system may be impossible, strategically planned experiments can dramatically reduce the resources required to completely map composition/processing space. We collaborate with experts to develop and deploy state of the art artificial intelligence methods to accelerate the discovery of material systems [1,2].

Combinatorial thin film libraries are created by reactively sputtering atoms from one or more targets onto a 4-inch silicon wafer, followed by processing the as-deposited material with a thermal treatment technique called laser spike annealing (LSA) in collaboration with the Thompson group (Figure 1). Co-sputtering in an off-axis geometry with two or more targets produces a monotonic gradient in chemical makeup of the thin film across the

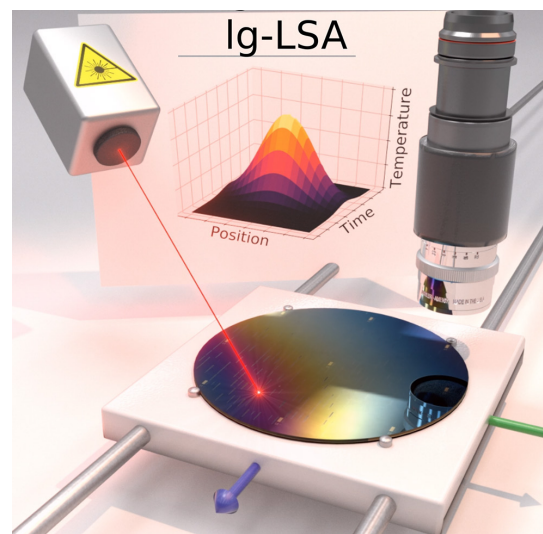


Figure 1: A rendering of the laser spike annealing experiment in relation to the as-deposited thin film and analytical methods.

substrate. Increasing the number of targets decreases the area on the film with unique composition; the trade-off of span in chemical space is the scarcity. LSA controls the peak temperature and duration at that temperature; i.e., the thermal history the material experiences. LSA can be localized to a 2 mm by 5 mm area on the wafer, allowing a regular grid of 616 independently chosen LSA conditions.

There are an additional nine locations photolithographically defined on the wafer that enable precise alignment among various spatially resolved techniques used to analyze the processed materials (e.g., optical microscopy, thin film reflectance spectroscopy, and spatially resolved x-ray diffraction characterization).

Figure 2 shows the layout of the annealed stripes on a composition spread and the total number of conditions for an example material system. To make the experimentation reproducible and precise (especially critical for automation and autonomous learning,) prior to thin film deposition every silicon wafer has the location grid and calibration marks lithographically patterned using CNF.

We successfully processed and characterized (see one example stripe in Figure 3) over 30 unique thin film metal oxide libraries at the Cornell High Energy Synchrotron Source in April 2022. Five of those libraries were used in successful active learning trials yielding a marked improvement in throughput of materials exploration and demonstrating integration of artificial intelligence into experimental materials research. Four of the other libraries were of interest for their electrical properties and further processed into a dense array of thin film capacitor devices which are currently being measured. The remainder of the combinatorial libraries are being analyzed and the most illuminating results are being prepared for publication. An example product from the x-ray characterization is the processing phase diagram in Figure 4.

Conclusions and Future Steps:

We have engineered an autonomous materials synthesis and characterization system for accelerating the discovery of novel materials. The reproducibility, reliability, and analytical requirements for automating the experimentation and incorporating the artificial intelligence was made possible by utilizing the CNF. Future research efforts will focus on improving the temporal and thermal calibration of the laser spike annealing method using lithographically patterned phase-change materials. One limitation of the post processed capacitor devices is the time required to exhaustively measure the properties each stripe of annealed material. We plan to employ artificial intelligence to optimally measure the minimum number of capacitors required to map structure/property relations by taking advantage of information derived from x-ray characterization. Developing this foundation will allow us to construct more complicated devices for assessing transport and carrier properties of the electronic materials.

References:

- [1] Ament, S., et al. *Sci. Adv.* 7, eabg4930 2021.
- [2] Sutherland, D., et al. *ACS Combi. Sci.* 2020, 22, 12, 887-894.

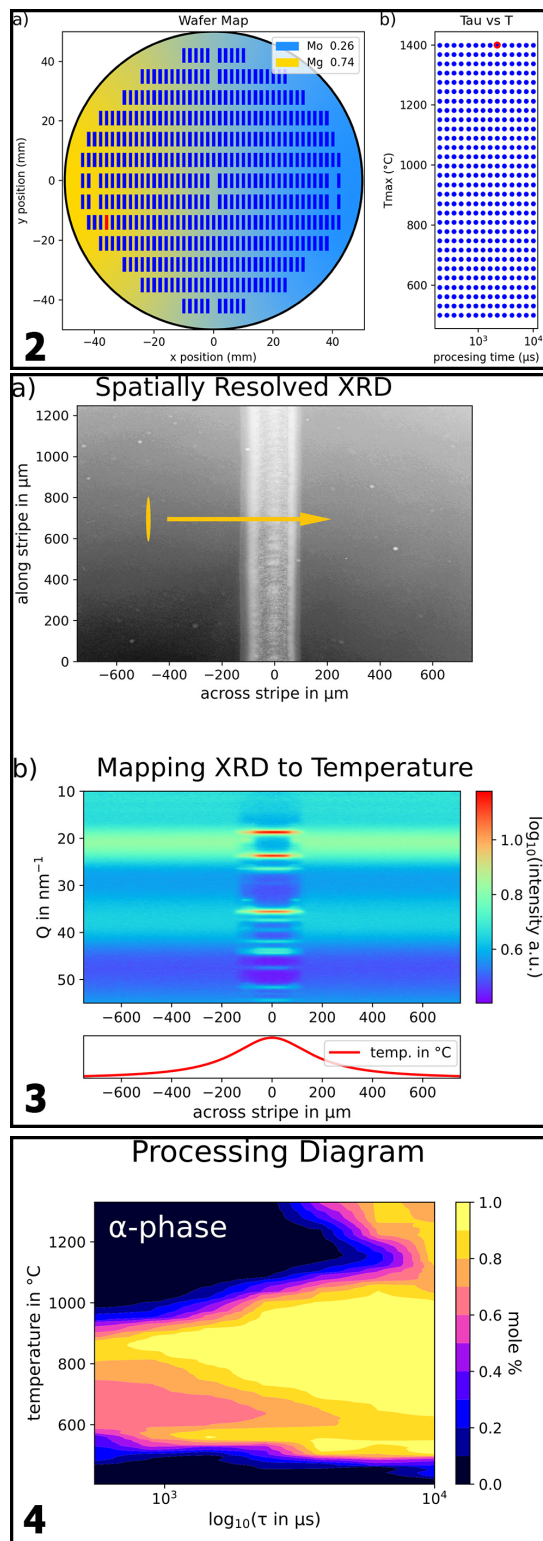


Figure 2, top: a) Cartoon description showing the distribution of laser spike annealing experiments over a 4" wafer with a pseudo binary composition spread of the cations Mg and Mo. b) Distribution of laser spike annealing conditions in the materials processing space. Figure 3, middle: a) Optical micrograph of a stripe of annealed material; yellow spot indicates the footprint and aspect ratio of the x-ray diffraction beam and arrow indicates direction of data collection. b) The spatially resolved x-ray diffraction heatmap comprised of the individual 1D diffraction patterns with the conversion of spatial extent to effective temp of annealing. Figure 4, bottom: A novel quantitative processing phase diagram for a laser spike annealed thin film oxide.

Low Loss Superconducting LC Resonator for Strong Coupling with Magnons

CNF Project Number: 2126-12

Principal Investigator(s): Gregory D. Fuchs

User(s): Qin Xu

Affiliation(s): Physics Department, Cornell University

Primary Source(s) of Research Funding: Center for Molecular Quantum Transduction (CMQT)

Contact: gdf9@cornell.edu, qx85@cornell.edu

Primary CNF Tools Used: AJA Sputter Deposition, Heidelberg Mask Writer - DWL2000, GCA 6300 DSW 5X g-line Wafer Stepper, YES Asher, AJA Ion Mill, P7 Profilometer, Zeiss Ultra SEM, DISCO Dicing Saw, Naby Nanometer Pattern Generator System (NPGS), Westbond 7400A Ultrasonic Wire Bonder

Abstract:

We design, fabricate and study an on-chip superconducting LC resonator that is strongly coupled to a magnon mode of the molecular ferrimagnet vanadium tetracyanoethylene (V[TCNE]_x). We demonstrate a fully integrated, lithographically defined photon-magnon hybrid quantum system in the strong coupling limit where all elements have low damping.

Summary of Research:

The goal of this research is to study a strongly coupled hybrid quantum device composed of a superconducting microwave resonator and a magnon mode. A key figure-of-merit is the cooperativity $C = 4g^2/K_m K_r$ between magnons and resonator photons, where g is the coupling strength between magnons and photons, and K_m , K_r are damping rate for magnons and resonator respectively. The two systems are strongly coupled if $C > 1$.

We use V[TCNE]_x as the magnetic material in this work because of its low Gilbert damping rate $\alpha \sim 10^{-4}$ and thus low K_m and because it can be grown on most materials and patterned via electron beam lithography. To increase the coupling g , we design an LC resonator with a small inductance and a narrow inductor wire. We pattern the V[TCNE]_x directly on the inductor wire of LC resonator.

We first designed the LC resonator based on a single layer of photolithography. We used KLayout to design the structure and ADS to simulate its microwave response. The simulation predicts a resonance frequency around 4.2 GHz. We then patterned the photomask with the Heidelberg Mask Writer - DWL2000.

The superconducting material for our device is niobium that we deposited on sapphire using the AJA Sputter

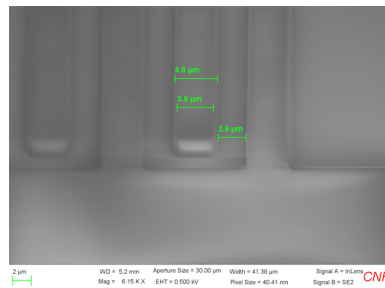


Figure 1: SEM image of the profile of resist after being exposed and developed.

Deposition (second tool) at 600°C. The resulting Nb thickness is around 60 nm measured with the P7 profilometer. It has a critical temperature (T_c) of 7.3 K. The high T_c of Nb and the low loss tangent of sapphire help limit the damping rate of the superconducting device.

We patterned the Nb using photolithography followed by dry etching. We spun LOR3a and then S1813 on the Nb with hotplate baking, exposed

the resists in GCA 6300 DSW 5X g-line stepper, and then developed the resist in MIF 726. The profile of the patterned resists was checked in Zeiss Ultra SEM. Figure 1 shows the SEM image of the patterned resists which looks perfect.

Then we descummed the developed resists in YES Asher, etched the Nb not covered by resist in AJA ion mill, and then put the wafer into the solution 1165 to strip off all the resists on the wafer. We patterned around 50 resonators on a 2-inch wafer. Because of the dust on the wafer during photolithography, around 20 of the devices have defects on their patterns, but the remaining 30 looked perfect under the microscope.

Before V[TCNE]_x deposition, we tested the resonator itself. For measurement setup, we cut the wafer and



Figure 2: The LC resonator device bonded to a chip carrier.

separated those 50 devices using the DISCO dicing saw, glued one of the resonators on a PC board with varnish and then used the Westbond 7400A Wire Bonder to wire-bond the device for microwave measurement.

Figure 2 shows a microscope image of the device wire bonded on the PC board.

With a vector network analyzer (VNA), we tested the resonator device in a He-3 cryostat at base temperature 0.43 K. The transmission spectrum of the frequency scan shows the resonator has a quality factor of 5031.

We use an electron-beam lithography liftoff process to template the growth of $V[TCNE]_x$. We spun the e-beam resist on the resonator chip and then exposed the resist in Nability Nanometer Pattern Generator System (NPGS). Figure 3 shows the device after being exposed in the NPGS, where vertical line of the T-shaped part is the inductor wire.

We then shipped the templated device to Ohio State University for collaborator Donley Cormode in Professor Ezekiel Johnston-Halperin's group for $V[TCNE]_x$ growth and liftoff. The dimension of the $V[TCNE]_x$ is $600 \mu\text{m}$ times $6 \mu\text{m}$ times 300nm .

We studied the integrated hybrid device at 0.43 K. We measured the microwave transmission coefficient using a vector network analyzer.

Figure 4 shows the transmission spectrum as a function of magnetic field and frequency. The avoided level crossing characteristic of a strongly coupled hybrid device is observed. We find the coupling coefficient is $g = 90.4 \text{ MHz}$, the resonator damping rate is $K_r = 0.90 \text{ MHz}$ and the magnon damping rate is $K_m = 33.3 \text{ MHz}$. Using these values, we find the cooperativity $C = 4g^2/K_m K_r = 1091$, which greatly exceeds 1.

Conclusions and Future Steps:

We have demonstrated the design and fabrication of a low loss superconducting on-chip LC resonator in the CNF cleanroom. Our device achieved strong coupling between $V[TCNE]_x$ magnons and resonator photons with a cooperativity greater than 1000. In this experiment the $V[TCNE]_x$ appeared inhomogeneously broadened (not limited by intrinsic damping). We may increase the cooperativity further by better understanding and controlling the mechanisms of $V[TCNE]_x$ linewidth at cryogenic temperatures.

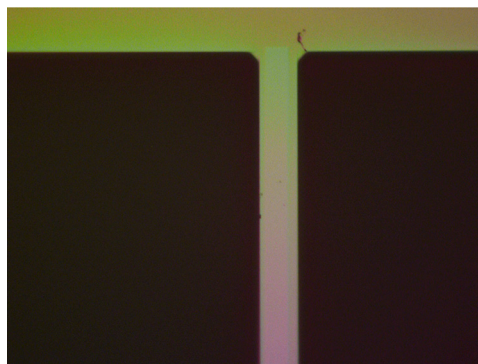


Figure 3: Microscope image of LC resonator device after being coated with e-beam resist and then being exposed in Nability. The T-shaped part represents the superconducting film, and the lighted vertical rectangle on the vertical line of the T-shaped part represents the Nability exposed area.

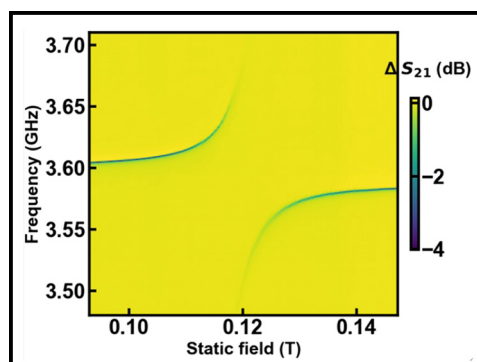


Figure 4: The transmission spectrum of field-frequency scan of the resonator-magnon system. The anti-crossing of the dip is the signature of coupling between resonator photons and $V[TCNE]_x$ magnons.

Encapsulation of Photocathodes in Two-Dimensional Materials

CNF Project Number: 2584-17

Principal Investigator(s): Melissa A. Hines

User(s): Qingyuan "Amy" Zhu, Dulanga Somaratne, Annabel Selino

Affiliation(s): Dept. of Chemistry and Chemical Biology, Cornell University

Primary Source(s) of Research Funding: Center for Bright Beams,
an NSF Science and Technology Center

Contact: Melissa.Hines@cornell.edu, qz337@cornell.edu,
dulanga.somaratne@cornell.edu, avs58@cornell.edu

Website: <https://mahines.github.io/HinesLab/>

Primary CNF Tools Used: SC4500 Odd-Hour Evaporator, Glen 1000 Resist Strip

Abstract:

We are developing a new technique for encapsulating highly reactive photocathodes in an atomically thin membrane that protects them from oxidation and degradation without affecting their photoemission properties or chemical purity.

Summary of Research:

Photocathodes are materials that eject electrons under illumination. By their very nature, high-performance photocathodes must be made from materials that lose electrons easily — in other words, materials that are easily oxidized. For example, many photocathodes are either coated with alkali metals (e.g., Cs/GaAs) or comprised of alkali metals (e.g., Cs₃Sb). This presents a technical challenge, as exposure to even trace amounts of O₂ or H₂O will destroy or degrade the photocathode. For highest performance, the photocathodes must also be atomically flat and extremely homogeneous.

To meet these challenges, we are developing a technique to produce photocathodes encapsulated in two-dimensional materials, such as graphene or hexagonal boron nitride. The key challenge in this project is ensuring that every step of the fabrication leaves no residue on the surface, as even monolayer levels of contamination could significantly reduce photoelectron transmission and beam brightness.

In the first step of fabrication, commercial two-dimensional materials, which are grown on a copper foil, are coated with a thin gold layer in the SC4500 thermal/e-beam evaporator. The two-dimensional material on the backside of the copper foil is then removed using 100W of oxygen plasma in the YES oxygen plasma asher. The copper foil is then removed with an aqueous etchant, allowing the graphene side of the gold-coated graphene to be adhered to a low energy substrate. The gold film is then removed by a second aqueous etch.

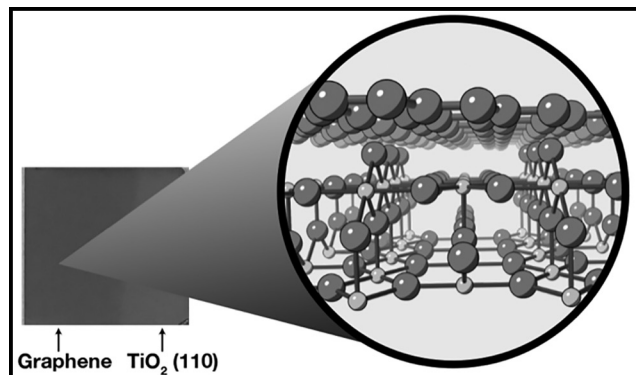


Figure 1: Optical image of TiO₂(110) with single-layer graphene on left side. The inset is a model of single-layer graphene on TiO₂(110).

Fabricating Superconducting Microwave Resonators for On-Chip Electron Spin Resonance Spectroscopy

CNF Project Number: 2705-18

Principal Investigator(s): Farhan Rana

User(s): Arjan Singh

Affiliation(s): Electrical and Computer Engineering, Cornell University
Primary Source(s) of Research Funding: Air Force Research Lab (AFRL)
Grant No. FA9550-18-1-0529

Contact: farhan.rana@cornell.edu, as2995@cornell.edu
Primary CNF Tools Used: AJA Sputter Deposition Tool,
ABM Contact Aligner, PT770 Etcher, DISCO Dicing Saw

Abstract:

Electron spin resonance (ESR) spectroscopy has been a useful tool for measuring defect spins in semiconductors [1-6]. We are utilizing the robust capabilities of the Cornell NanoScale Facility (CNF) to develop an ESR spectrometer with the capability to measure defect spins in MBE-grown films as thin as 100 nm. Here, we demonstrate a planar microwave resonator, the principal device to be used in the spectrometer, fabricated using the superconducting metal niobium (Nb). The superconducting metal allows us to shrink the dimensions of our device by a hundred times, compared to a copper resonator, while avoiding any kind of resistive loss. This allows us to simultaneously benefit from a high quality-factor (Q -factor) and a small spatial extent of the microwave-spin interaction.

Summary of Research:

Electron spin resonance (ESR) spectroscopy is based on exploiting the Zeeman interaction between a magnetic field and a spin. Ever since it was proposed to study nuclear spins nearly a century ago [8], it has been a useful tool to study spins in materials (1-7).

A (non-oscillating) magnetic field splits degenerate spin states by an energy, $E = \gamma_s B$ (assuming spin-1/2 particles), where γ_s is the gyromagnetic ratio (the ratio between the magnetic moment of a particle to its angular momentum) and B is the applied magnetic field. The energy E for magnetic fields on the order of 1 T can easily be supplied by microwaves of frequencies, $f \sim 1$ -10 GHz.

Thus, the essential idea of ESR spectroscopy is that by supplying microwave radiation to semiconductor samples subject to a magnetic field, we can induce transitions between spin states of defects when the condition, $hf = \gamma_s B$ is met, where h is Planck's constant.

By observing these transitions, we can extract the gyromagnetic ratio, γ_s , associated with a defect-spin state, giving us insight into its electrical/magnetic properties. Figure 1 shows a schematic of such an ESR experiment.

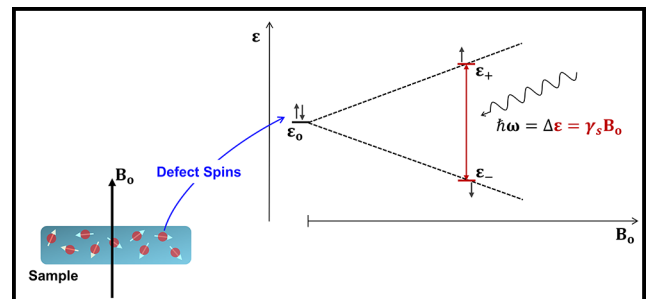


Figure 1: Schematic showing the basic principle of electron spin resonance (ESR) spectroscopy.

ESR spectrometers, by and large, use a 3-D microwave resonator to deliver microwaves to samples subject to a DC magnetic field. 3-D microwave resonators, owing to their large magnetic field mode volumes, are not sensitive to MBE grown thin films. Using a 2-D, planar microwave resonator we can minimize the magnetic field mode volume, and thus minimize the magnetic field fill factor (represents the fraction of magnetic field seen by the film being probed). A small magnetic fill factor (close to unity) will allow us to probe defect spins in

semiconductor films as thin as ~ 10 nm. The key to a high magnetic fill factor is shrinking the dimensions of the resonator. However, small dimensions also mean higher resistive losses in metals. We use the superconducting metal Nb, to overcome this trade-off, thus maintaining a high magnetic fill-factor and near-zero resistive loss [9]. The small mode volume of a 2-D planar resonator also means that much of the magnetic field is within the substrate on which the resonator is patterned. To minimize the dielectric loss resulting from this, we use a sapphire substrate, owing to sapphire's small loss-tangent and high dielectric constant.

Methods and Results:

We used the Cornell NanoScale Facility (CNF) to fabricate this superconducting 2D resonator. Figure 3a shows the fabrication procedure for our devices. We sputter deposit 100 nm of Nb. We measured the temperature dependent resistance of this film and found the superconducting transition temperature T_c to be ~ 6 K. Since we will be conducting our experiments in a 4.2 K liquid He cryostat, this T_c will work well for our experiments. Figure 4 shows the critical dimensions of the fabricated device.

Conclusion and Future Steps:

The next step is to measure the transmission through the fabricated resonators and measure the Q -factor. This will be followed by an ESR measurement of MBE grown thin films of ultrawide-bandgap semiconductor β -Ga₂O₃.

Acknowledgements:

I would like to thank the CNF staff, without whom this work would not have been possible and will not be able to continue. I especially thank Tom Pennell, Chris Alpha, Aaron Windsor, Garry Bordonaro, and Jeremy Clark for their invaluable input and support.

References:

- [1] M Baeumler, et al., J. Phys. C: Solid State Phys. 20 L963 (1987).
- [2] W. E. Carlos, et al., Phys. Rev. B 48, 17878 (1993).
- [3] J H N Loubser and J A van Wyk, Rep. Prog. Phys. 41 1201 (1978).
- [4] W. V. Smith, et al., Phys. Rev. 115, 1546 (1959).
- [5] B. E. Kananen, et al., Applied Physics Letters 110, 202104 (2017).
- [6] Nguyen Tien Son, et al., Applied Physics Letters 117, 032101 (2020).
- [7] Conrad Clauss, et al., J. Phys.: Conf. Ser. 592 012146 (2015).
- [8] G. Breit and I. I. Rabi, Phys. Rev. 38, 2082 (1931).
- [9] A. Bienfait, et al., Nature Nanotechnology, volume 11, pages 253–257 (2016).

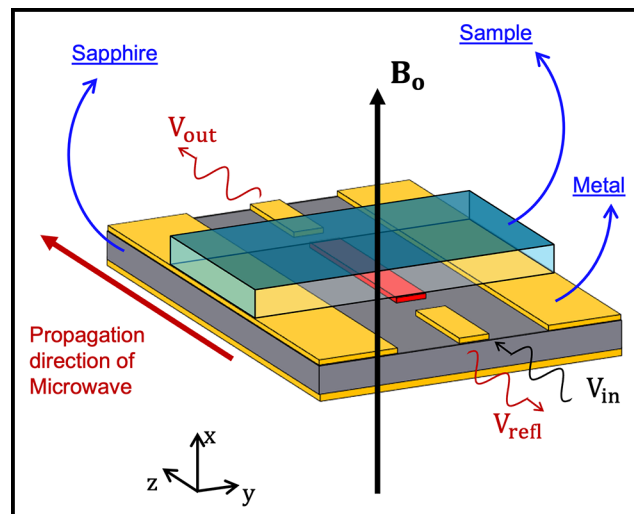


Figure 2: Basic layout of our ESR measurement. The planar microwave resonator lies at the heart of the setup and is fabricated at the Cornell NanoScale Facility (CNF).

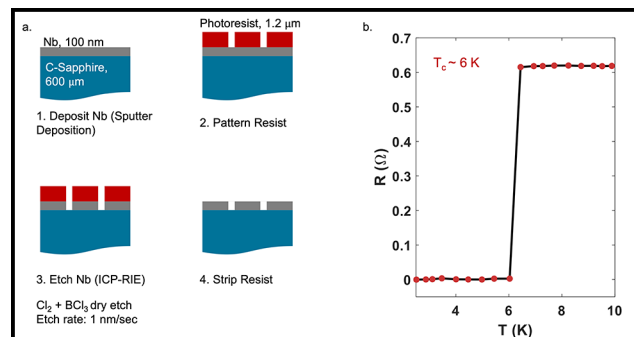


Figure 3: (a) Shows the schematic of the fabrication process used to fabricate our microwave resonator. (b) Shows Resistance vs. Temperature of our deposited Nb film.

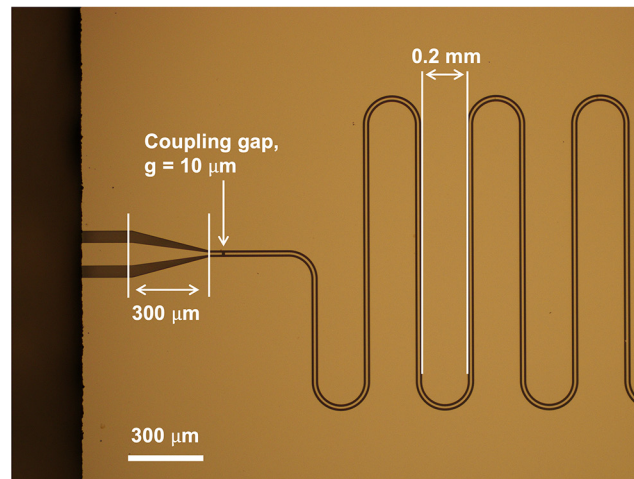


Figure 4: Key dimensions of the fabricated superconductor microwave resonator.

Investigation of Palladium Strains and Actuation in Gaseous Environments

CNF Project Number: 2736-18

Principal Investigator(s): Nicholas L. Abbott¹

User(s): Hanyu (Alice) Zhang²

Affiliation(s): 1. Smith School of Chemical and Biomolecular Engineering,
2. School of Applied and Engineering Physics; Cornell University

Primary Source(s) of Research Funding: Cornell Center for Materials Research
with funding from the National Science Foundation Materials Research
Science and Engineering Centers program (DMR-1719875)

Contact: nla34@cornell.edu, hz496@cornell.edu

Primary CNF Tools Used: Heidelberg Mask Writer - DWL2000, ABM Contact Aligner, Oxford
81/82/100 Etchers, AJA Sputter Deposition Tool, AJA Ion Mill, Oxford PECVD, SC4500
Odd-Hour Evaporator, PT770 Etcher (Left Side), OEM Endeavor Aluminum Nitride
Sputtering System, Leica CPD300 Critical Point Dryer, DISCO Dicing Saw

Abstract:

We are developing a palladium-based microactuator that is driven by hydrogen as a fuel. After an initial delay upon exposure to hydrogen, these actuators exhibit high strains within a short time period. In this report, we show the fabrication process of these devices, present the characterization of simple hinge structures, and discuss initial results.

Summary of Research:

We are interested in understanding palladium as a material that can be used to drive the actuation of microscopic hinges for use in micro robotics. Palladium is a metal known for its high hydrogen affinity, and the palladium hydride system is well-studied [1]. For this project, we are utilizing palladium's high affinity to hydrogen to obtain actuation on the microscale. By inducing an asymmetric strain across the thickness of a bimorph made with palladium and an inert material (currently using titanium), we have observed curling and bending in these devices.

To fabricate these devices, a sacrificial layer of aluminum nitride is initially sputtered onto a fused silica wafer with the OEM Endeavor tool and patterned. Then a layer of titanium sputtered, and a layer of palladium is evaporated onto the sample to create a Ti-Pd bimorph of various thicknesses. This bimorph is patterned and etched with the Ion Mill. To selectively control where the bimorph bends, silicon dioxide panels that are around 500nm thick are deposited with plasma enhanced chemical vapor deposition on the Oxford PECVD and etched with a mixture of trifluoromethane and oxygen plasma on the Oxford 100. We then soak the chips in 726 MIF developer to release the devices and use the Leica critical point dryer to dry the chips.

After the devices are made, we bring them into the lab to test inside a gas chamber.

Conclusions and Future Steps:

Figure 1 shows some example devices that we are currently testing. After an initial delay upon exposure to hydrogen, these devices respond rapidly and show high strain (Figure 2). We also observed that this process is reversible (Figure 3).

To understand palladium's interaction with hydrogen in our microactuators, we are planning various experiments in which critical dimensions of the palladium microactuators will be varied. We will also perform imaging of the deposited palladium before, during and after exposure to gaseous environments.

References:

- [1] Dekura, S., Kobayashi, H., Kusada, K., and Kitagawa, H. (2019). Hydrogen in Palladium and Storage Properties of Related Nanomaterials: Size, Shape, Alloying, and Metal-Organic Framework Coating Effects. *ChemPhysChem*, 20(10), 1158-1176.

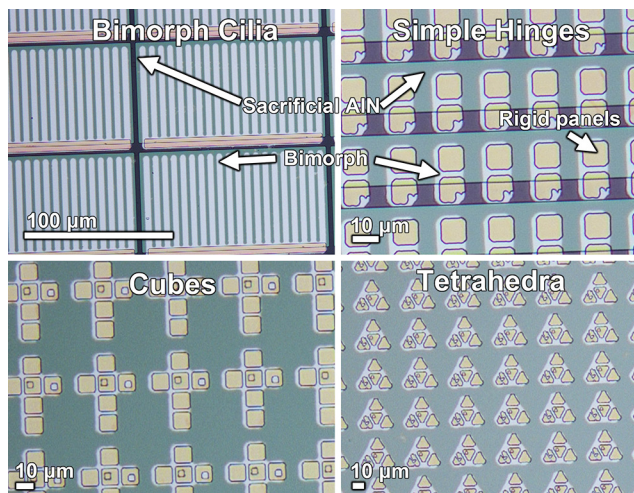


Figure 1: Example collection of devices pre-release.

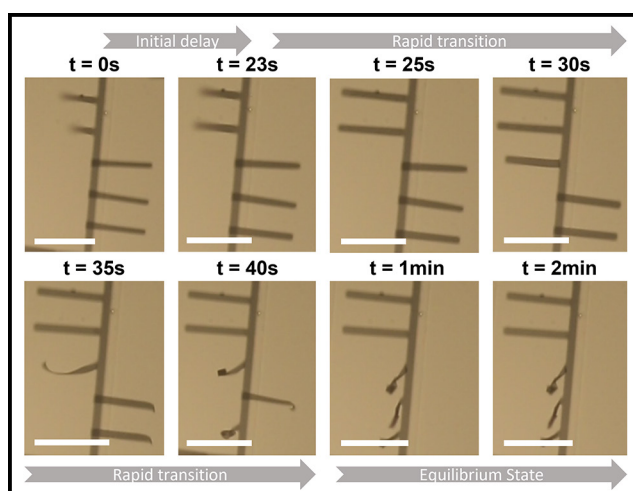


Figure 2: Time-lapse photos showing palladium's response to hydrogen using simple cilia-like microactuator devices. The microactuators consist of 3.5 nm of sputtered titanium and 7.6 nm of evaporated palladium, both deposited as a bilayer. Scale bars are 50 μm .

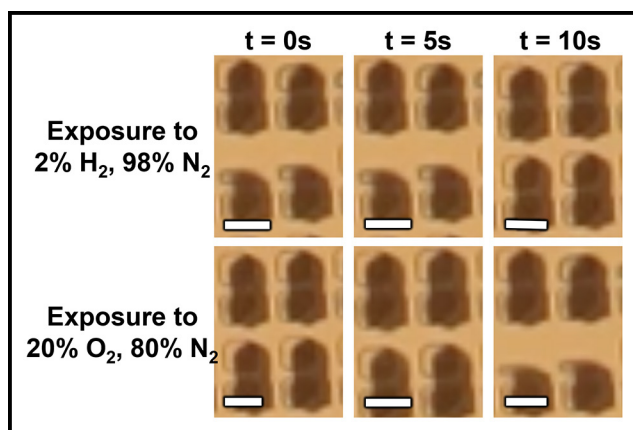


Figure 3: Time-lapse photos showing bilayer hinges exposed to a hydrogen environment and then air. Scale bars are 10 μm . The bilayer hinge consists of 10 nm of sputtered titanium and 20 nm of evaporated palladium. The panels are fabricated from 420 nm of SiO_2 . A 20 nm layer of titanium is used to adhere the palladium and SiO_2 layers.

Scissionable Polymer Photoresist for Extreme Ultraviolet Lithography

CNF Project Number: 2751-18

Principal Investigator(s): Christopher Kemper Ober

User(s): Jingyuan Deng

Affiliation(s): Materials Science and Engineering, Cornell University

Primary Source(s) of Research Funding: INTEL Corporation

Contact: c.ober@cornell.edu, jd966@cornell.edu

Primary CNF Tools Used: ASML 300C DUV Stepper,
JEOL 6300 E-Beam Lithography, P10 Profilometer

Abstract:

Scissionable polymers are polymers that will depolymerize under different stimuli including acid, base, and free radicals. These polymers have been investigated in the development of photoresists and other degradable materials. This work focuses on the poly(phthalaldehyde), PPA, a family of scissionable polymers. The PPA backbone consists of acetal linkages that are very sensitive to acids. Upon exposure to acids, the polymer chain depolymerizes to its corresponding monomers. This depolymerization behavior makes PPAs excellent candidates as photoresist materials. Several new PPA photoresists are being explored in this work.

Summary of Research:

Poly(phthalaldehyde) (PPA) is a well-established depolymerizable photoresist developed by IBM in 1983 [1]. Monomer outgassing and absence of bench-stability resulted in the resist being abandoned in favor deprotection based resists. However, multiple groups have recently explored the potential of PPA under EUV exposure [2-4], but so far success has been elusive. In comparison with other depolymerizable systems, a very limited number possess the same depolymerization kinetics, and those that do suffer from poor sensitivity or outgassing.

The difficulty in simultaneously maximizing resolution, line edge roughness, and sensitivity is known as the RLS trade-off and is one of the foremost issues hampering EUV performance. One accepted technique to bypass the RLS trade-off is to employ high loadings of photoacid generator (PAG) and in the process diminish deleterious shot noise effects. Unfortunately, the popular ionic PAGs phase separate regularly at elevated concentrations, especially above 20 wt%. Non-ionic PAGs present a potential solution to this problem as they can remain miscible at significantly higher concentrations compared to ionic PAGs. These PAGs also possess advantages in dark loss and acid yield when exposed to e-beam.

Despite the potential of non-ionic PAGs, they are consistently inferior to ionic PAGs in terms of sensitivity, with few able to achieve the requisite EUV dose-to-clear under 20 mJ/cm². This challenge has been worsened by the dearth of mechanistic information available concerning the behavior of non-ionic PAGs under EUV exposure.

In this report, we describe the development and photolithographic performance of photoresists consisting of a PPA derivative and a non-ionic PAG. We found that many simultaneously possessed high stability and remarkable EUV sensitivity.

Results and Discussions:

Photoresist polymers (35 mg) and photoacid generators (7 mg) were dissolved in 1 mL propylene glycol methyl ether acetate (PGMEA). The resist was spin-coated onto a silicon wafer at 3000 rpm for 1 min. The coated silicon wafers were then exposed using ASML 300C DUV stepper. After exposure, the exposed film was baked and developed. The resulting line-space patterns were characterized using AFM shown in Figure 1.

As seen from these figures, the relatively rough line edge roughness was caused by the acid diffusion, which could be alleviated by changing the chemical structure of the photoacid generator.

We further investigated these resist materials under EUV exposure. By using these non-ionic PAGs, we were able to achieve dose to clear for as low as 12 mJ/cm².

Summary:

In summary, preliminary results were obtained with chain scissionable photoresists. With these results in hand, the lithographic performance of newly developed functionalized PPAs will be investigated.

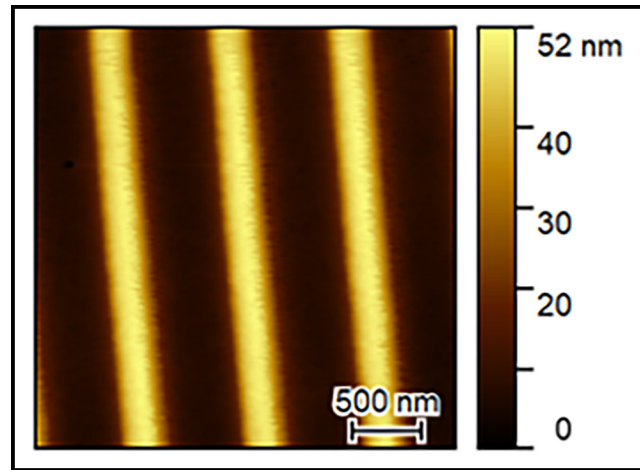


Figure 1: Line-space patterns characterized using AFM.

References:

- [1] H. Ito, C. G. Willson, *Polym. Eng. Sci.*, Chemical amplification in the design of dry developing resist materials, 1983, 23, 1012-1018.
- [2] A. Rathore, I. Pollentier, S. S. Kumar, D. De Simone, S. De Gendt, *J. Micro/Nanopattern. Mats. Metro.*, Feasibility of unzipping polymer polyphthalaldehyde for extreme ultraviolet lithography, 2021, 20, 034602.
- [3] P. A. Kohl, A. Engler, C. Tobin, C. K. Lo, *Journal of Materials Research*, Influence of material and process parameters in the dry-development of positive-tone, polyaldehyde photoresist, 2020, 35, 2917-2924.
- [4] J. Deng, F. Kaefer, S. Bailey, Y. Otsubo, Z. Meng, R. Segalman, C. K. Ober, *J. Photopol. Sci. Technol.*, New Approaches to EUV Photoresists: Studies of Polyacetals and Polypeptoids to Expand the Photopolymer, 2021, 34, 71-74.

Design and Fabrication of Integrated Magnetic Elastomer-Based Soft Actuator

CNF Project Number: 2866-20

Principal Investigator(s): Amal El-Ghazaly¹

User(s): Ludovico Cestarollo², Rodolfo Cantu³, Karthik Srinivasan¹

Affiliation(s): 1. Electrical and Computer Engineering, Cornell University; 2. Materials Science and Engineering, Cornell University; 3. Summer 2022 CNF REU Intern, Mechanical Engineering, The University of Texas at Austin

Primary Source(s) of Research Funding: National Science Foundation, 2022 CNF REU Program NSF Grant NNCI-2025233

Contact: ase63@cornell.edu, lc942@cornell.edu, rodolfo.cantu@utexas.edu, ks934@cornell.edu
Website: <https://vesl.ece.cornell.edu>

Primary CNF Tools Used: Heidelberg Mask Writer - DWL2000, ABM Contact Aligner, Hamatech Hot Pirana/Wafer Processor Develop, PT 72, C&D SmartProP9000, DISCO Dicing Saw, AFM - Veeco Icon, P7 Profilometer, RC2 Woollam Ellipsometer

Abstract:

Technological advancements to date have primarily focused on stimulating only two of the five human senses: sight and hearing. Touch-based interactive technologies can still be considered to be in their infancy. Haptic devices allow tactile interactions between humans and digital interfaces in many different arenas such as user interfaces for assisted and autonomous driving [1] and teleoperation [2]. Magnetorheological elastomers (MREs) based on nanoparticles constitute a promising candidate material for creating tactile interfaces capable of creating high-resolution features on the micron scale [3,4]. These magneto-responsive elastomers must be integrated with magnetic controls to create the local magnetic fields necessary to actuate deformations. Such a system composed of a magneto-responsive soft material and integrated magnetic controls has not been developed to date.

In order to highlight the potential for these devices, a process was developed to create a system of micromagnetic controls integrated into free-standing microscale cantilevers and beams. First, magnetic microscale circular and elliptical pillars were developed via sputtering and photolithography utilizing a lift-off process. These structures were utilized to create magnets with magnetic moments pointing respectively in the direction perpendicular and parallel to their surface. The magnetic properties of the deposited magnets were studied via vibrating sample magnetometry and the optimal dimensions for both geometries were identified. Based on simulation results, the optimally fabricated circles and ellipses were then deposited in pairs at different distances from each other. These systems of magnets were ultimately designed to be integrated into cantilevers and beams made of a micrometer thin nanoparticle-based MRE to create a magnetic soft actuator.

Summary of Research:

First, sets of micromagnets were fabricated with two geometries in order to preferentially set the anisotropy (direction of the magnetic moments) along two specific directions. Contact photolithography, sputtering, lift-off and argon ion milling (see Figures 1 and 2) were used to fabricate the magnets. Pillars with a circular base were developed to create magnets with perpendicular magnetic anisotropy (PMA), so with magnetic moments pointing in the thickness direction of the pillars. Pillars with an elliptical base were instead developed to create magnets with in-plane magnetic anisotropy (IMA), so with magnetic moments pointing in a direction lying

on the base of the pillars. The effect of the size of the magnets on their magnetic properties was investigated by depositing sets of magnets of different sizes on a wafer and then cutting the wafer into dies, with each die having a set of magnets with specific geometry and dimensions. These dies were then tested in a vibrating sample magnetometer to record magnetic hysteresis loops (magnetization vs. magnetic field). For the PMA magnets, pillars having a circular base with 5 μm diameter were determined to be optimal, since they yield a remanent to saturation magnetization almost equal to 1 and a large coercivity of about 1000 Oe.

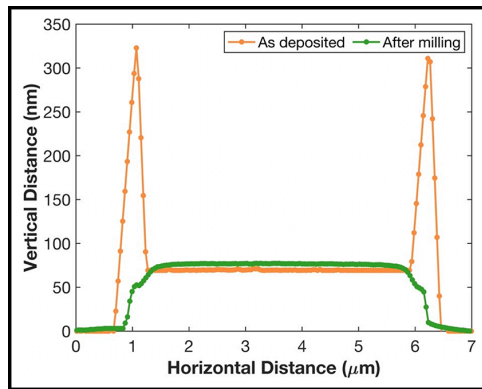


Figure 1: 2D AFM profile of 5 μm diameter circular pillar as deposited and after argon ion milling of the “rabbit ears”.

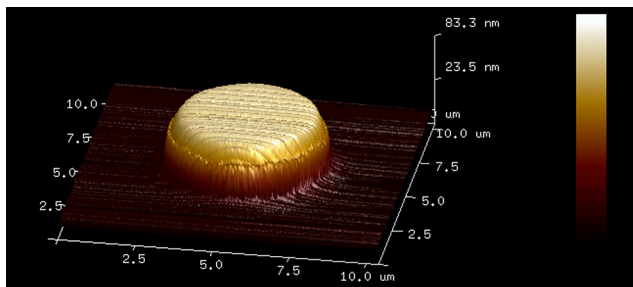


Figure 2: 3D AFM image of 5 μm diameter circular pillar after argon ion milling, showing smooth edges and absence of “rabbit ears” characteristic of lift-off process using deposition via sputtering.

For the IMA magnets, elliptical pillars with long and short axes dimensions of 3 and 15 μm were chosen as the optimal ones. This size allows to better tune the magnetic anisotropy in the direction of the long axis of the pillar (with larger sizes the difference between the loops recorded along the short and long axes of the pillars becomes less pronounced).

In order to obtain a soft magnetic elastomer with magnetic controls able to actuate deflections, we designed a system composed of a magnetorheological elastomer and the two optimally fabricated micromagnets described above (Figure 3 illustrates the device in the case of a simply supported beam). By having a PMA and an IMA magnet on the surface on a magneto-responsive material, the two magnets can couple with each other with magnetic flux lines penetrating into the material. Based on magnetic simulations performed in COMSOL Multiphysics, the two magnets were spaced 1, 1.5 and 2 μm away from each other (Figure 4 shows the 1.5 μm spacing case). These spacings guarantee strong coupling between IMA and PMA magnets so that the flux generated by the IMA magnet closes into the PMA one, creating a strong field extending into the elastomer. This magnetic flux closure generates a magnetic field gradient in proximity of the gap between the two magnets, which in turn causes the magnetic particles embedded into the elastomer to move towards where the flux is stronger, forcing the magnetic elastomer to deform.

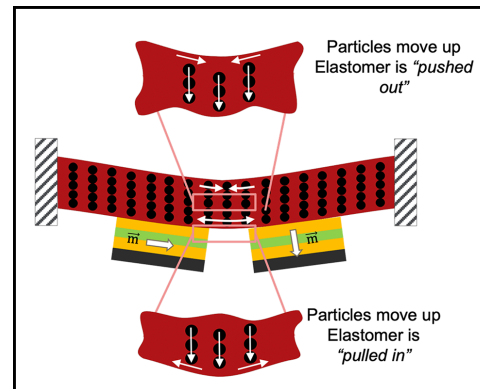


Figure 3: A magnetic soft actuator in the form of a simply supported beam. The two micromagnets generate the local fields that cause the deflection of the magnetic elastomer.

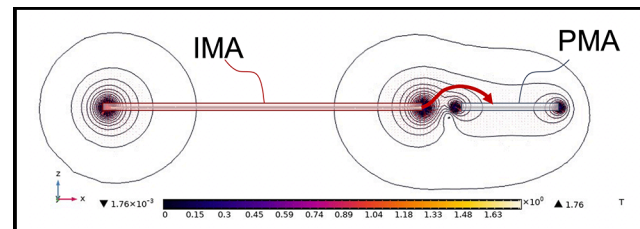


Figure 4: Magnetic simulation of IMA and PMA magnets spaced 1.5 μm away from each other. The contour lines show the change in magnitude of the magnetic flux density. The red arrow emphasizes the direction of magnetic flux closure from the IMA to the PMA magnet.

Conclusions and Future Steps:

We have successfully fabricated micro-sized magnets with perpendicular (PMA) and in-plane (IMA) magnetic anisotropy. In the case of PMA magnets, circular pillars were selected as the geometry of choice and an optimal diameter of 5 μm was determined. On the other hand, in the case of IMA magnets, elliptical pillars were selected as the geometry of choice and optimal long and short axes dimensions of 3 and 15 μm were selected.

PMA and IMA magnets were then fabricated on a wafer with spacings of 1, 1.5 and 2 μm between them. Simulations results indicated that such spacings allow the magnetic flux from the IMA magnet to couple with the PMA one. The next steps will require embedding these sets of micromagnets into a thin (2 μm thick) magnetic elastomer and shape this into beams to test their actuation performance.

References:

- [1] Terken, J; Levy, P; Wang, C; Karjanto, J; Yusof, N; Ros, F; Zwaan, S; Advances in Human Factors and System Interactions; Nunes, I. L., Ed.; Springer International Publishing, 2017; pp 107-115.
- [2] Hayward, V; Astley, O; Cruz-Hernandez, M; Grant, D; Robles-De-La-Torre, G; Sensor Review 2004, 24, 16-29.
- [3] L. Cestarollo, S. Smolenski, A. El-Ghazaly; ACS AppMats and Interfaces 14 (2022) 19002-19011. doi:10.1021/acsami.2c05471
- [4] Böse, H.; Gerlach, T.; Ehrlich, J. of Intelligent Material Systems and Structures 2021, 0, 1-15.

Fabrication of Microwells to Host Liquid Crystals (LCs) for Studies Aimed at Understanding the Coupling of Surfactant Concentration Gradients with LC Ordering

CNF Project Number: 2874-20

Principal Investigator(s): Nicholas L. Abbott

User(s): Soumita Maiti

Affiliation(s): Chemical and Biomolecular Engineering, Cornell University

Primary Source(s) of Research Funding: National Science Foundation (CBET-1803409 and EFMA1935252), Army Research Office through W911NF-15-1-0568 and W911NF-17-1-0575

Contact: nla34@cornell.edu, sm2766@cornell.edu

Website: <https://nlabbotcornell.weebly.com/>

Primary CNF Tools Used: Heidelberg Mask Writer, ABM Contact Aligner, DISCO Dicing Saw

Abstract:

We have used the CNF to fabricate microwells to host liquid crystals (LCs) in studies aimed at understanding how surfactant concentration gradients impact the LC ordering. Specifically, microwells with various shapes were fabricated by patterning SU-8 on glass surfaces using photolithography. LCs were dispensed into the microwells to create LC domains with diverse shapes. We have discovered that the optical responses of the LC films depend strongly on the LC domain shape.

Summary of Research:

We used photolithography to fabricate microwells with a depth of $\sim 20 \mu\text{m}$ and lateral dimensions ranging from $50 \mu\text{m}$ to $500 \mu\text{m}$. SU-8 25 was used as the photoresist. The ABM contact aligner was employed for UV exposure of the films of SU-8 on glass wafers through a chrome mask written using the Heidelberg Mask Writer - DWL2000. The wafers were cut in the shape of microscope slides ($75 \text{ mm} \times 25 \text{ mm}$) using the dicing saw. After treating the microwells with octadecyltrichlorosilane, we dispensed thin films of nematic LCs (5CB; Figure 1a) in them and attached them to the floor of a milli-fluidic channel (Figure 1c; detailed elsewhere [1]). A gradient in surfactant concentration (sodium dodecyl sulfate (SDS; Figure 1b)) was generated within the milli-fluidic channel by pumping two aqueous solutions containing different concentrations of SDS through the channel inlets under conditions of laminar flow (Figure 1c).

In response to a given external gradient in concentration of SDS, we observed the LC films to exhibit bright shape-dependent optical responses as presented in Figure 2. Although Figure 2 reveals a qualitatively similar progression of LC interference colors in the y-direction (direction of predicted SDS gradient) across each sample, independent of the shape of the LC film, the maximum optical retardance of the LC films and the width of the optically dark (extinct) bands were noted to differ significantly with a change in shape of the LC films.

We made systematic changes to the shapes of the LC films (lateral to the external gradient), ranging from the initial rectangular shapes to triangular shapes. We found that a select set of shapes generated a strong optical response (higher optical retardance) as presented in Figure 3. An inverted triangular shape (Figure 3 k-n) appears to be the LC domain shape that generates the strongest optical response.

In addition, we used rectangular LC films (prepared in rectangular microwells) to investigate how the non-equilibrium ordering of LCs driven by external gradients in surfactant concentration leads to the formation of localized assemblies of microparticles (Figure 4). Specifically, silica microparticles (diameter $3 \mu\text{m}$), initially present in the bulk 5CB, were driven to the aqueous-LC interface and formed localized chains at the middle of the interface when placed in a milli-fluidic channel containing a gradient in SDS concentration.

References:

- [1] Roh, S.; Tsuei, M.; Abbott, N. L. Using Liquid Crystals for *in situ* Optical Mapping of Interfacial Mobility and Surfactant Concentrations at Flowing Aqueous-Oil Interfaces. *Langmuir* 2021, 37 (19), 5810–5822. <https://doi.org/10.1021/acs.langmuir.1c00133>.

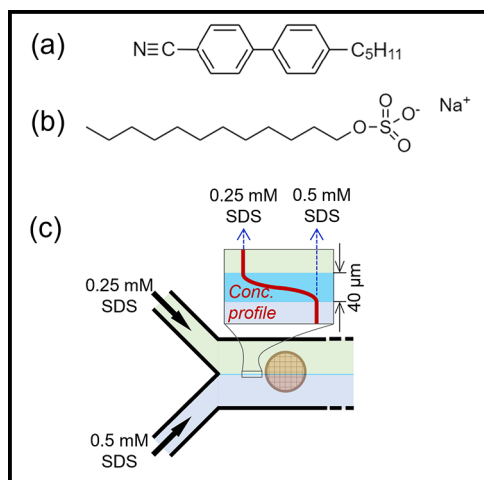


Figure 1: Molecular structure of (a) 4-Cyano-4'-pentylbiphenyl (5CB) and (b) Sodium dodecyl sulfate (SDS). (c) Aqueous solutions of SDS at 0.25 mM and 0.5 mM concentrations (color-coded as green and blue, respectively) are passed through two inlets of the milli-fluidic channel at a flow rate of 2 mL/min each. The concentration profile of SDS near the middle of the channel width is illustrated in the inset.

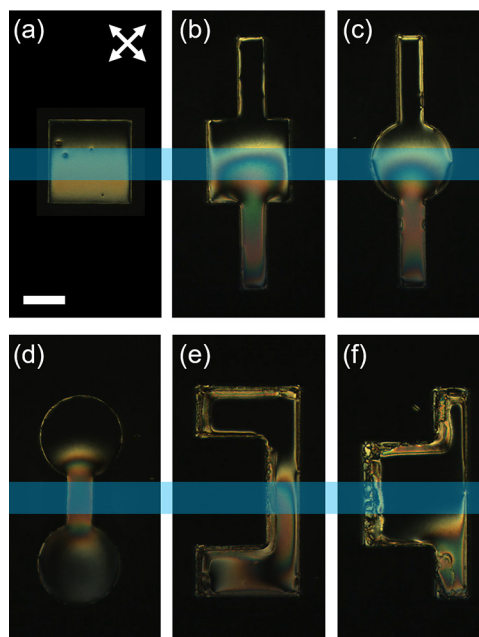


Figure 2: Optical response of 5CB confined in microwells of different shapes to a gradient in SDS concentration generated by pumping solutions of 0.5 mM and 0.25 mM SDS in 300 mM NaCl at a flow rate of 0.5 mL/min each. The blue bands passing through the middle of the films represent the position of the external gradient. Scale bar is 100 μm .

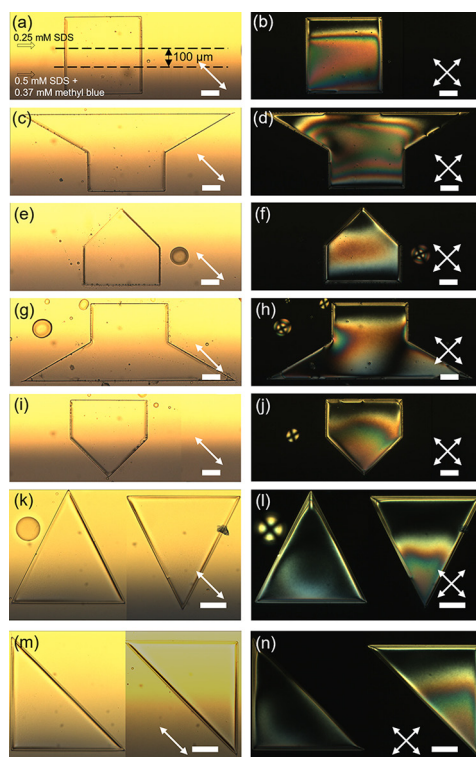
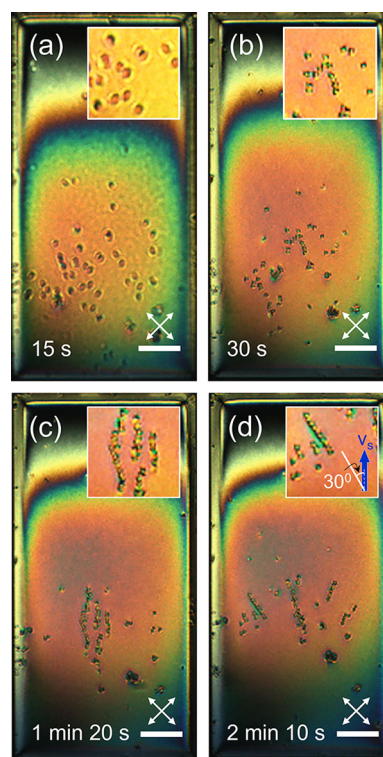


Figure 3, left: 0.25 mM SDS solution is pumped through one inlet and a solution containing 0.5 mM SDS and 0.37 mM methyl blue is pumped through the other inlet of the channel at a flow rate of 0.5 mL/min each. (a, c, e, g, i, k, m) Bright-field images of LC confined in microwells of different shapes. Black dotted lines in (a) represent the extent of the imposed gradients in the bulk aqueous solution. (b, d, f, h, j, l, n) Optical response of LC between cross polars. Scale bars are 100 μm . Figure 4, right: A film of 5CB with dispersed silica particles is placed inside a milli-fluidic channel containing a gradient in SDS concentration generated by pumping solutions of 0.5 mM and 0.25 mM SDS in 300 mM NaCl at a flow rate of 0.5 mL/min each. Insets show magnified views of the organizations of particles in the time series images. Scale bars are 50 μm .



Sizing Thermo-responsive Colloidal Particles with Dynamic Light Scattering

CNF Project Number: 2949-21

Principal Investigator(s): Jerome Fung

User(s): Jerome Fung, Emily Leach

Affiliation(s): Department of Physics and Astronomy, Ithaca College, Ithaca, NY

Primary Source(s) of Research Funding: American Chemical Society – Petroleum Research Fund

Contact: jfung@ithaca.edu, eleach@ithaca.edu

Primary CNF Tools Used: Malvern Zetasizer Nano

Abstract:

We are synthesizing transparent, thermo-responsive core-shell colloidal particles for use as a model system in studies of the glass transition. The particles consist of an optically-dense polystyrene core surrounded by a nearly-transparent poly-N-isopropylacrylamide shell. We use dynamic light scattering (DLS) to measure the size of the particles during and after their preparation. We also use DLS to examine the response of the core-shell particles to temperature changes.

Summary of Research:

Understanding the mechanical behavior of glasses, which have liquid-like structure but solid-like moduli, is an important open question in condensed matter physics. Colloidal suspensions are useful as model systems for studying condensed-matter phenomena like the glass transition. Specifically, colloidal particles can be used as “model atoms” that can be engineered to exhibit interactions similar to those in atomic systems, but are large enough to be directly visualized in real space using optical microscopy.

Recently, Perro and co-workers introduced a core-shell particle that could potentially be useful as a model system for studying glasses [1]. The particles consist of a small, optically-dense, mechanically-rigid core surrounded by a thermo-responsive, nearly-transparent, soft hydrogel shell (Figure 1). These particles are expected to have

soft-sphere interactions, which may be more relevant to atomic systems than colloidal particles with hard-sphere interactions, which have been much more extensively studied. The particles reversibly deswell when heated above room temperature, which would allow the particle volume fraction, a key thermodynamic parameter, to be tuned *in situ*. Finally, since the shells are nearly refractive index-matched in water, it is possible to image deep within dense suspensions using techniques such as confocal microscopy. Our overall goal is to measure the interactions between these core-shell particles and how the interactions affect the rheology of dense suspensions of the particles.

First, however, we need to synthesize the particles since they cannot be purchased commercially. Measuring particle sizes with dynamic light scattering (DLS) using the Malvern Zetasizer Nano at CNF is important in the synthesis. We need to know both the size of the cores alone as well as the size of the completed core-shell particles. We also need to measure the temperature dependence of the shell size.

The Zetasizer is useful for these measurements for several reasons. DLS is particularly appropriate for sizing our particles: because our cores are smaller than the optical diffraction limit and the shells are nearly-index matched, sizing the particles by direct optical imaging would not be effective, and electron microscopy would most likely destroy them. In addition, the Zetasizer allows us to easily regulate the sample temperature over the relevant range (25-40°C). Finally, we can also use

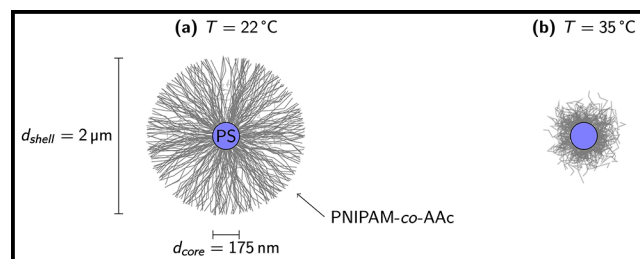


Figure 1: Schematic illustration of core-shell polymer particles characterized using dynamic light scattering. The particles consist of a polystyrene (PS) core surrounded by a thermo-responsive poly-N-isopropyl acrylamide/acrylic acid (PNIPAM-co-AAc) shell. At room temperature, the shells are highly swollen and nearly index-matched in water. At higher temperatures, the shells collapse.

the intensity autocorrelation functions measured in DLS to determine whether or not the particles are monodisperse.

Figure 2 shows two intensity autocorrelation functions, one for cores alone and one for completed core-shell particles. The autocorrelation functions exhibit an exponential decay characteristic of monodisperse suspensions. Notably, the longer decay time scale for the core-shell particles indicates that they are larger than the bare cores as expected. Moreover, fitting a refined model based on a cumulant expansion of the particle size distribution to the measured autocorrelation functions allows us to quantify the particle size as well as estimate the small but nonzero polydispersity index of the suspensions [2].

While the core-shell particles we have prepared thus far have not exhibited the expected thermoresponsive behavior, we are currently working to optimize the synthesis reaction parameters. We expect DLS measurements with the Zetasizer at CNF to remain an important part of our ongoing work.

References:

- [1] A. Perro, G. Meng, J. Fung, and V. N. Manoharan, "Design and synthesis of model transparent aqueous colloids with optimal scattering properties." *Langmuir*, 25 (19), 11295-11298 (2009).
- [2] B. J. Frisken, "Revisiting the method of cumulants for the analysis of dynamic light-scattering data." *Applied Optics*, 40 (24), 4087-4091 (2001).

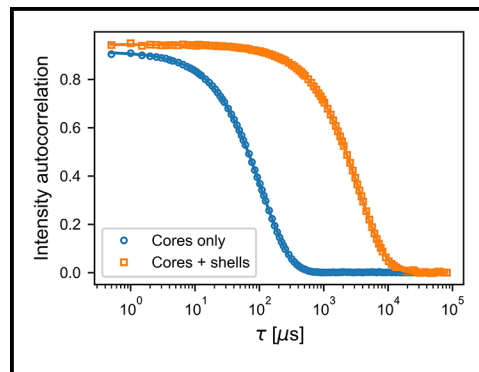


Figure 2: Intensity autocorrelation functions measured for cores only (blue circles) and core-shell particles (orange squares). Solid lines are fits to a second-order cumulant model for the particle size distribution [2]. The autocorrelation function for the core-shell particles decays over a longer time scale than the autocorrelation function for the cores only, indicating that the core-shell particles are larger than the cores alone as expected.

Measuring the Conductivities of Ionic and Metal Ligand Coordinated Polymers

CNF Project Number: 2952-21

Principal Investigator(s): Meredith Silberstein

User(s): Max Tepermeister

Affiliation(s): Sibley School of Mechanical and Aerospace Engineering, Cornell University

Primary Source(s) of Research Funding: Defense Advanced Research Projects Agency

Contact: meredith.silberstein@cornell.edu, mt845@cornell.edu

Website: silbersteinlab.com

Primary CNF Tools Used: SC4500 Evaporator, ABM Contact Aligner, Heidelberg Mask Writer

Abstract:

Ionic polymers are a new class of material that promise to enable deformable computers and bio-compatible electronics. We developed a gold on glass experimental electrode setup with built-in spacers using photolithographic tools. We then used this setup to characterize a wide range of ionic polymers and discovered some unexpected trends in their behavior, including an increase in conductivity with ion size.

Summary of Research:

The primary goal of this research project is to discover circuit elements describing synthetic soft materials that utilize ionic transport. This work is funded through a Defense Advanced Research Projects Agency Young Faculty Award.

Circuit design to date has been primarily based upon metal and semiconductor substrates—inherently hard materials with features that have minimal similarity to or compatibility with biosystems. Biosystems have a diverse set of highly nonlinear and environmentally responsive features within underlying circuitry (e.g., neurons, membrane ion channels) that operate via ion transport and storage. While these systems have been extensively studied within biomechanical contexts, few reduced-order circuit models have been developed. Moreover, soft ionic conducting material development has primarily been focused on maximizing conductivity for use as electrochemical conversion and storage device membranes. As a result of the foregoing prevailing conditions, progress in wetware has been limited: hampered by the disparate knowledge bases.

As part of this broader effort, we are experimentally characterizing the ionic conductivity of a wide range of polymers. These electrochemical impedance spectroscopy and cyclic voltammetry experiments are conducted on a Gamry 3000AE in the Silberstein lab with either a 2-wire standard or 4-wire Kelvin measurement.

It is critical for the accuracy and repeatability of these experiments that the electrodes be non-reactive and that the distance between electrodes and electrode area be set at a constant value.

Utilizing CNF tools, we built a gold on glass electrode using a liftoff process that meets all our requirements. We patterned S1800 series photoresist onto fused quartz 100 mm wafers, then deposited a 10 nm titanium adhesion layer followed by a 100 nm gold layer via electron-beam thermal evaporation. The photoresist and excess gold was then removed using the water-jet liftoff machine. We then photo-patterned 5 μm and 10 μm thick SU-8 spacers on the periphery of the electrodes.

Some of the materials we test are viscous liquids, so we designed the spacers in a sparse grid to allow for the test materials to flow out of the test cell. A diagram and image of these devices are shown in Figure 1 and 2 respectively. The SU-8 spacer can be seen in Figure 2 as the small lighter rectangles in a square around the central gold square.

In order to perform impedance spectroscopy measurements, sample material is dropped on one of these electrodes and a second electrode is clamped on top, rotated by 180°. The central 1 cm^2 squares of gold overlap and create a parallel plate capacitor. By applying

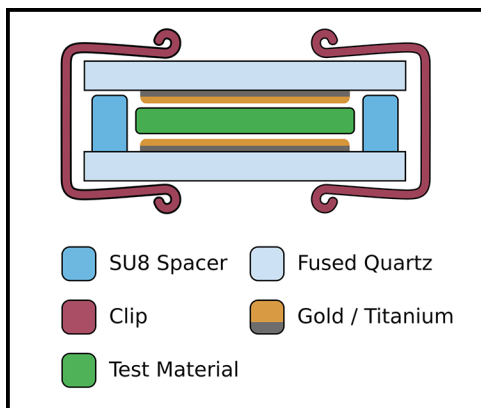


Figure 1: Diagram of experimental setup.



Figure 2: One electrode out of four on a wafer.

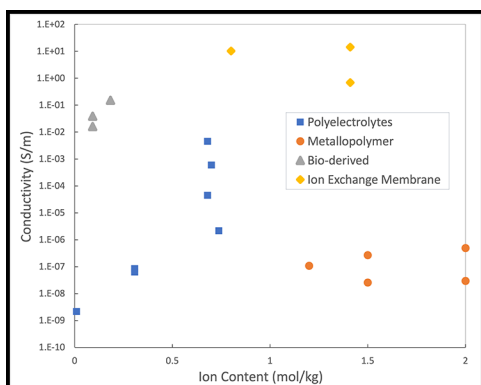


Figure 3: Conductivity vs. ion content for four material classes.

oscillating electric fields at various frequencies, we can precisely characterize the electrical response of our test material. This electrochemical testing fixture has been applied to testing metal ligand coordinated polymers, polyionic hydrogels, and ionomers swollen with ionic liquids. Figure 3 shows the ionic conductivity of a wide range of materials that we have characterized, mainly with this device.

With PDMS, we have found that the ionic conductivity of ligand functionalized PDMS with metal salts incorporated far exceeds the conductivity of unfunctionalized PDMS. Further, the conductivity of metallo-PDMS depends on both the type of anion and cation within the added salt and on the concentration of the salt. Interestingly, larger anions lead to higher conductivity despite expected size effects on their diffusivity because they associate less strongly with the metal cation. Advantageously, these larger anions are also able to be incorporated into the polymer at larger concentrations without precipitating into crystallites. We also found that by using more than one cation type, we could partially de-couple viscosity and conductivity. With the polyionic hydrogels and ionomers, we have used the test setup to characterize their basic electrical response, and are in the process of characterizing the properties of various material junctions. These junctions promise to give current rectifying behavior in a way similar to semiconductor diodes.

Conclusions and Future Steps:

The tools at the CNF were instrumental in creating a precise and repeatable experimental setup for our material characterization, leading us to surprising conclusions about the behavior of some ionic systems. In the coming year, we are interested in moving beyond single material characterization and towards device/junction characterization. Many proposed devices require length scales on the order of microns in order to function effectively. As such, one possible way to make these devices is by patterning positive and negative ionomers themselves using photolithographic techniques, which we hope to explore in the near future.

Magnetic Polymer-Grafted Nanoparticles

CNF Project Number: 2955-21

Principal Investigator(s): Christopher Kemper Ober

User(s): Chenyun Yuan

Affiliation(s): Department of Materials Science and Engineering, Cornell University
Primary Source(s) of Research Funding: About Air Force Office of Scientific Research
Contact: cko3@cornell.edu, cy479@cornell.edu
Primary CNF Tools Used: Malvern Nano ZS Zetasizer, DISCO Dicing Saw,
Rame-Hart 500 Goniometer, Scanning Electron Microscope

Abstract:

In this project, polymer-grafted nanoparticles with various magnetic cores (Fe_3O_4 , CoFe_2O_4 , etc.) and different polymer canopies are synthesized. The magnetic interactions among cores and the chemical forces (hydrogen bond, ionic interactions, etc.) among polymer brushes are assumed to affect the self-assembly property of the nanoparticles. The self-assembly structures (monolayers, superlattices, etc.) of the particles are made on silicon wafers and other substrates for further study. The polymer canopies would not only modify the surface properties of the metal oxide nanocores to prevent them from aggregating, but also introducing tunable chemical forces into the polymer-graft nanoparticles self-assembly structures.

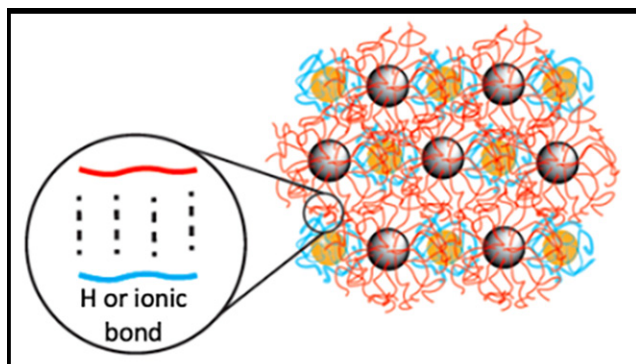


Figure 1: Demonstration of the inter-particle hydrogen bonding or ionic interactions.

Summary of Research:

Polymer-grafted nanoparticles (PGNs) have received increasing attention because they possess the advantages of both the grafted polymer and inorganic cores, and thus demonstrate superior optical, magnetic, electronic, and catalytic properties. One potential application for PGNs is the formation of self-assembly structures and as a building block for the development of photonic/optical/magnetic devices. Thus, PGNs with tailorable interparticle interactions, via either inorganic magnetic cores (magnetic interactions) or polymer brush chemistry (hydrogen bonds, ionic interactions, etc.) (Figure 1), are indispensable for the formation of a superlattice with a defined and ordered structure.

A combined approach of mini-emulsion polymerization and surface-initiated Atom Transfer Radical Polymerization will be used to make the PGNs [1]. To couple the initiator molecules and the metal oxide surface, a silane-based coupling agent is used. The surface-initiated Atom Transfer Radical Polymerization is carried out by adding appropriate combination of ligand, copper, monomer, reducing agent, and shuttling agent. The emulsion is prepared by Pluronic F-127, a non-ionic surfactant. The PGN self-assembly structures are fabricated using multiple techniques, including Langmuir-Blodgett method and simply drop-casting. The morphology of PGNs and order of the self-assembly structure are characterized by scanning electron microscope (SEM), transmitting electron microscope (TEM), scanning transmission electron microscopy (STEM), and atomic force microscope (AFM), and the magnetic properties are characterized using Physical Property Measurement System (PPMS). Besides these, many facilities in CNF would help this research project.

For example, the Malvern Nano ZS Zetasizer will be helpful for characterizing the size of synthesized particles. To study the magnetic properties of the particle self-assembly, we need to cut silicon wafers into 2 mm × 2 mm square pieces precisely, and the DISCO Dicing Saw can help us doing this. The polymer-grafted nanoparticles with different polymer canopies are mixed in the self-assembly structure, and the Energy-dispersive X-ray Spectrometer will help us see which polymer corona is around the particles. Also, we may

characterize the surface modified by those particles, so facilities like contact angle would be very helpful.

An example HAADF-STEM image of polymethyl methacrylate-grafted Fe₃O₄ nanoparticles is shown in Figure 2. The polymer chains are entangled together and form a thick shell around the particle cores. Because of the low electron scatter ability of the polymers, the polymer shell is transparent than the inorganic crystal cores.

In conclusion, polymer-grafted nanoparticles with various polymer chemistries and different magnetic core materials are synthesized using a grafting-from approach. The self-assembly structures of these PGNs are made using several techniques. While we are getting some promising initial results that are showing the potential of these magnetic PGNs for fabricating self-assembled structures, further research is still needed to optimize the inter-particle interactions and tune the self-assembling behaviors. In future, the effect of the size, the polymer composition, and graft density, etc., will be studied.

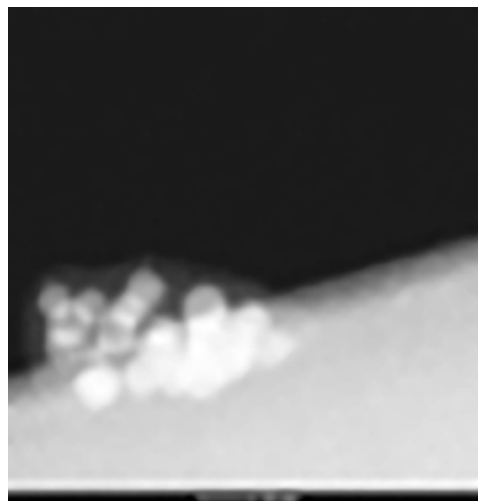


Figure 2: An example HAADF-STEM image of PMMA-grafted Fe₃O₄ cores.

References:

- [1] Yuan, C., Käfer, F., and Ober, C. K. (2021). Polymer-Grafted Nanoparticles (PGNs) with Adjustable Graft-Density and Interparticle Hydrogen Bonding Interaction. *Macromolecular Rapid Communications*, 43(12), 2100629. <https://doi.org/10.1002/marc.202100629>.
- [2] Oh, J. K., and Park, J. M. (2011). Iron oxide-based superparamagnetic polymeric nanomaterials: Design, preparation, and biomedical application. *Progress in Polymer Science*, 36(1), 168-189. <https://doi.org/10.1016/j.progpolymsci.2010.08.005>.

Tracking the TaS₂ Charge Density Wave Transition with Electron Microscopy and Electric Biasing

CNF Project Number: 2967-21

Principal Investigator(s): Judy J. Cha

User(s): James L. Hart, Saif Siddique

Affiliation(s): Department of Materials Science and Engineering, Cornell University, Ithaca NY

Primary Source(s) of Research Funding: Gordon and Betty Moore Foundation

Contact: jc476@cornell.edu, jlh487@cornell.edu, ms2895@cornell.edu

Primary CNF Tools Used: Nability Lithography System, Zeiss Supra SEM, CHA Thermal Evaporator

Abstract:

Our project's aim is to better understand the charge density wave (CDW) and associated metal to insulator transition (MIT) in 2-dimensional crystals of tantalum disulfide (TaS₂). We use *in situ* cryogenic scanning transmission electron microscopy (STEM) with *in situ* electric biasing to correlate changes in the CDW properties and sample resistance as a function of temperature. While this project is still on going, we have reached several milestones, including detecting the CDW and MIT with electrical resistance measurements, and developing a novel STEM strategy to track the CDW transition in real space. This project involves electron beam lithography and thin film deposition performed at the CNF.

Summary of Research:

Tantalum disulfide (TaS₂) crystals with the 1T crystal structure undergo a CDW transition at ~ 150 K from the so-called nearly commensurate (NC) to the fully commensurate (C) phases, and there is an associated MIT with a ~ 10-fold increase in resistance. Importantly, the transition can be driven via an electric pulse, which allows for the operation of 2-terminal devices for neuromorphic computing [1]. However, our understanding of how the CDW transition occurs in real space is very limited, both for transitions driven by thermal cycling and with electric pulses. To address this question, we use a novel variable temperature STEM holder, which allows for continuously variable temperature from ~ 100-1000 K, and also permits measurement of sample resistance *in situ* [2]. In principle, this approach will allow us to visualize changes in the CDW structure as a function of temperature, which we can then correlate with changes in the sample resistance. Moreover, we will be able to visualize the CDW during electric pulsing.

The first step towards this goal is to fabricate TaS₂ devices and measure the CDW / MIT *ex situ* (meaning outside of the STEM). To do so, we first exfoliated TaS₂ flakes onto a SiO₂ / Si substrate. We then used the Nability electron lithography package on the Supra scanning electron microscope (SEM) to lithographically pattern electrodes onto the flake. Lastly, we used the CHA thermal evaporator to deposit Cr / Au electrodes. An example device is shown in Figure 1.

Electrical resistance versus temperature data is shown in Figure 2 for another device. The measurement was performed using a physical property measurement system. The thermally induced CDW transition is clearly observed.

Having successfully measured the CDW transition in flakes *ex situ*, our next goal was to observe the transition with *in situ* STEM. For these experiments, we used specialty SiNx substrates with pre-patterned electrodes and through-holes for STEM observation. Figure 3 shows a TaS₂ flake which we transferred onto the pre-patterned electrodes. Note the hole underneath the flake, which is used for STEM imaging. We then studied this device within the STEM. Figure 4 shows a STEM image of the same flake, and the inset shows an electron diffraction pattern, which encodes information related to the CDW structure. By analyzing the diffraction data, we are able to determine the nature of the CDW phase.

Conclusions and Future Steps:

In this project we have fabricated TaS₂ electronic devices, and observed the CDW transition using electrical measurements. We have also developed a STEM method to observe the CDW transition in real space with nanoscale spatial resolution. Next steps for this project will include imaging the CDW phase with STEM, both as a function of temperature and applied electric field.

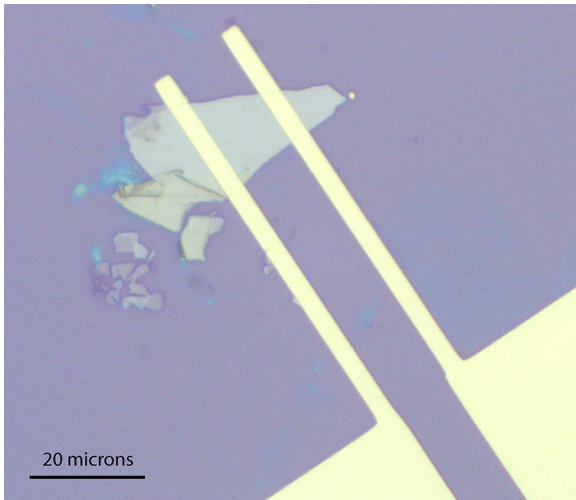


Figure 1: Optical image of a TaS_2 flake exfoliated onto SiO_2/Si , with Cr / Au electrodes patterned on top of the flake.

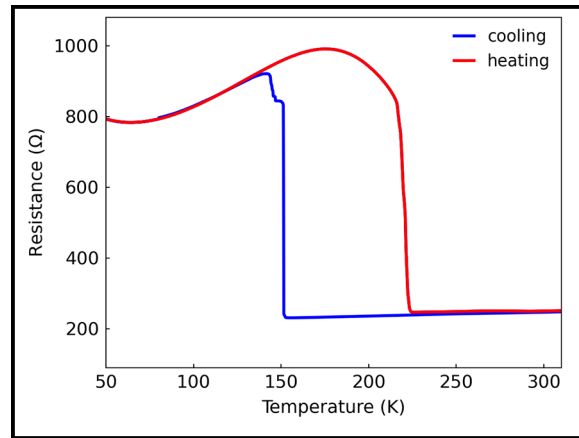


Figure 2: Resistance versus temperature data for a 2-terminal TaS_2 device.

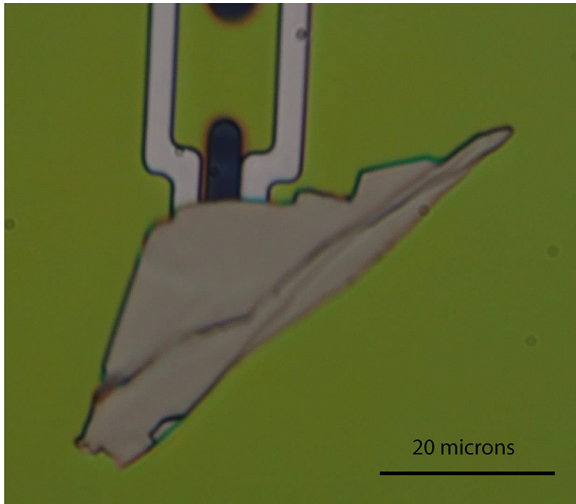


Figure 3: Exfoliated TaS_2 transferred to a chip that allows for in situ STEM measurements. The dark hole beneath the flake allows for STEM observation, and the electrodes allow for in situ biasing.

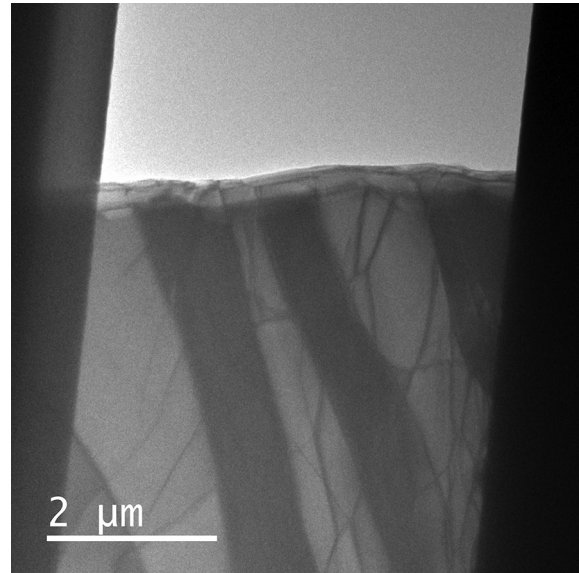


Figure 4: Same TaS_2 flake shown in Figure 3, but imaged within the STEM. The dark bands on the left and right hand sides of the image are the electrodes, and the empty region at the top of the image is the through-hole. The inset shows an electron diffraction pattern, and the weaker spots correspond to the CDW.

References:

- [1] Hollander, M. J.; Liu, Y.; Lu, W.-J.; Li, L.-J.; Sun, Y.-P.; Robinson, J. A.; Datta, S. Electrically Driven Reversible Insulator-Metal Phase Transition in $1\text{T}'\text{-TaS}_2$. *Nano Lett.* 2015, 15 (3), 1861-1866.
- [2] Goodge, B. H.; Bianco, E.; Schnitzer, N.; Zandbergen, H. W.; Kourkoutis, L. F. Atomic-Resolution Cryo-STEM Across Continuously Variable Temperatures. *Microsc. Microanal.* 2020, 26 (3), 439-446.

Photolithographic Patterning of Alignment Fiducials for X-Ray Nano-Diffraction

CNF Project Number: 2989-21

Principal Investigator(s): Andrej Singer

User(s): Aileen Luo

Affiliation(s): Materials Science and Engineering, Cornell University

Primary Source(s) of Research Funding: National Science Foundation, Department of Energy

Contact: asinger@cornell.edu, al2493@cornell.edu

Primary CNF Tools Used: Heidelberg Mask Writer – DWL 2000,
Hamatech Mask Chrome Etch, ABM Contact Aligner

Abstract:

Alkaline fuel cells and electrolyzer cells are promising alternative forms of energy conversion and storage devices due to their potential for eliminating the need for precious-metal catalysts. Epitaxially grown transition metal oxide thin films have demonstrated promising activity for the oxygen reduction reaction [1], the rate-limiting step for catalysis in alkaline fuel cells. To better understand localized structural and electronic changes in the catalyst under operating conditions, we aim to study them using x-ray nano-diffraction and x-ray absorption near-edge structure at the hard x-ray nanoprobe beamline at the National Synchrotron Light Source II.

Summary of Research:

Focusing of x-rays to a 25 nm spot on a sample requires alignment fiducial markers with sharp edges of less than half a micron in width. Using the computer-aided design software L-Edit and the Heidelberg Mask Writer – DWL2000, we designed and wrote a 5-inch photomask with multiple configurations of the pattern shown in Figure 1. Using S1800 series positive tone photoresist and the ABM Contact Aligner, we transferred the pattern onto samples of sizes 5 mm × 5 mm and 10 mm × 10 mm. DC magnetron sputtering (Cornell Center for Materials Research) was used to deposit 10 nm of titanium and 50 nm of copper metal onto the samples. Sonication in acetone was used to lift off the excess metal and complete the process.

Conclusions and Future Steps:

The fabrication of alignment features was completed successfully and tested at the hard x-ray nanoprobe beamline. For future measurements, we will design and make proof-of-concept devices at the Cornell NanoScale Facility for a three-electrode electrochemical cell compatible with the limitations of the beamline.

References:

[1] Y. Yang, et al. J. Am. Chem. Soc. 2019, 141, 1463-1466.

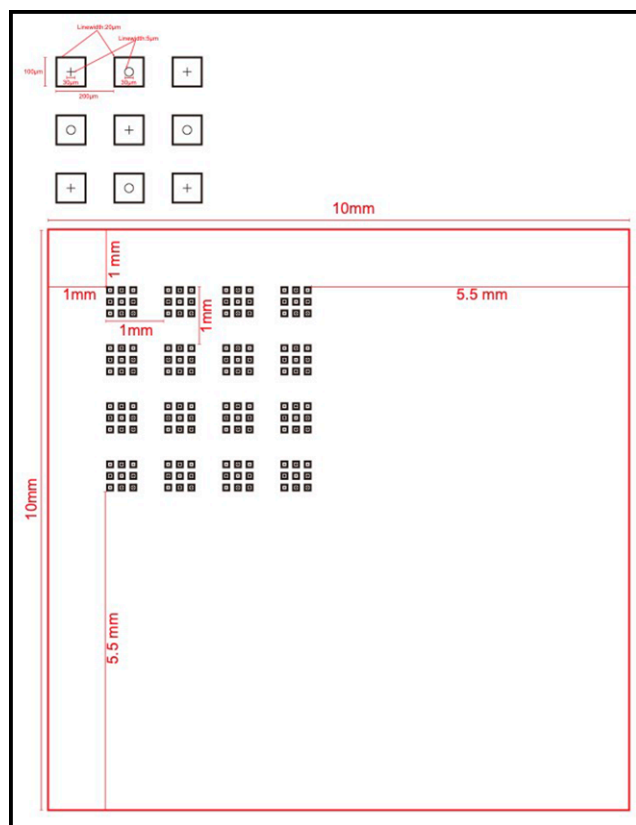


Figure 1: Schematic credit to Dr. Ludi Miao. Arrays of circles and crosses contained in larger squares.

